Simulation of Global Land Surface Conditions from 1948 to 2004. Part I: Forcing Data and Evaluations

TAOTAO QIAN, AIGUO DAI, KEVIN E. TRENBERTH, AND KEITH W. OLESON

National Center for Atmospheric Research, Boulder, Colorado*

(Manuscript received 4 February 2005, in final form 22 February 2006)

ABSTRACT

Because of a lack of observations, historical simulations of land surface conditions using land surface models are needed for studying variability and changes in the continental water cycle and for providing initial conditions for seasonal climate predictions. Atmospheric forcing datasets are also needed for land surface model development. The quality of atmospheric forcing data greatly affects the ability of land surface models to realistically simulate land surface conditions. Here a carefully constructed global forcing dataset for 1948–2004 with 3-hourly and T62 (~1.875°) resolution is described, and historical simulations using the latest version of the Community Land Model version 3.0 (CLM3) are evaluated using available observations of streamflow, continental freshwater discharge, surface runoff, and soil moisture. The forcing dataset was derived by combining observation-based analyses of monthly precipitation and surface air temperature with intramonthly variations from the National Centers for Environmental Prediction–National Center for Atmospheric Research (NCEP–NCAR) reanalysis, which is shown to have spurious trends and biases in surface temperature and precipitation. Surface downward solar radiation from the reanalysis was first adjusted for variations and trends using monthly station records of cloud cover anomaly and then for mean biases using satellite observations during recent decades. Surface specific humidity from the reanalysis was adjusted using the adjusted surface air temperature and reanalysis relative humidity. Surface wind speed and air pressure were interpolated directly from the 6-hourly reanalysis data. Sensitivity experiments show that the precipitation adjustment (to the reanalysis data) leads to the largest improvement, while the temperature and radiation adjustments have only small effects.

When forced by this dataset, the CLM3 reproduces many aspects of the long-term mean, annual cycle, interannual and decadal variations, and trends of streamflow for many large rivers (e.g., the Orinoco, Changjiang, Mississippi, etc.), although substantial biases exist. The simulated long-term-mean freshwater discharge into the global and individual oceans is comparable to 921 river-based observational estimates. Observed soil moisture variations over Illinois and parts of Eurasia are generally simulated well, with the dominant influence coming from precipitation. The results suggest that the CLM3 simulations are useful for climate change analysis. It is also shown that unrealistically low intensity and high frequency of precipitation, as in most model-simulated precipitation or observed time-averaged fields, result in too much evaporation and too little runoff, which leads to lower than observed river flows. This problem can be reduced by adjusting the precipitation rates using observed-precipitation frequency maps.

1. Introduction

Historical records of surface evaporation, runoff, soil moisture, and other land surface fields are unavailable over most of the continents. For example, there have been no direct measurements of actual evaporation or evapotranspiration over most land areas. Records of soil moisture are available only for a few regions and often are very short in length (Robock et al. 2000). Surface runoff is not measured and is often estimated using simple water balance models (e.g., Fekete et al. 2002). While streamflow has been monitored by gauges along many of the world's major rivers, the publicly available records of streamflow are incomplete and often short in length (Dai and Trenberth 2002), and the number of streamflow gauges has been declining during

* The National Center for Atmospheric Research is sponsored by the National Science Foundation.

Corresponding author address: Dr. Taotao Qian, National Center for Atmospheric Research, P.O. Box 3000, Boulder, CO 80307-3000.
E-mail: tqian@ucar.edu

recent decades (Shiklomanov et al. 2002). The lack of historical data of land surface fields hampers our ability to study the variability and changes in these variables and interactions among them (Ziegler et al. 2002). Moreover, these data are needed for verifying and initializing numerical weather and climate models (Dirmeyer et al. 1999).

Land surface fields from atmospheric and climate models such as the National Centers for Environmental Prediction–National Center for Atmospheric Research (NCEP–NCAR) (Kalnay et al. 1996) and the European Centre for Medium-Range Weather Forecasts (ECMWF) (Uppala et al. 2005) reanalyses are not suitable for climate studies because they are affected by large errors in model-simulated precipitation (Higgins et al. 1996; Janowiak et al. 1998; Trenberth and Guillemot 1998; Betts et al. 2003, 2005; Ruiz-Barradas and Nigam 2005), clouds (Trenberth et al. 2001a), and other atmospheric forcing (Berg et al. 2003). For example, large biases have been identified in reanalysis evapotranspiration (Lenters et al. 2000; Ruiz-Barradas and Nigam 2005), runoff and streamflow (Roads and Betts 2000; Betts et al. 2003, 2005), and snow and soil moisture (Lenters et al. 2000; Maurer et al. 2001). A major cause of these biases, in addition to the precipitation errors, is the use of soil moisture "nudging" or adjustment, which results in nonclosure of the surface water budget (Maurer et al. 2001).

Recently, large efforts have been devoted to simulate past land surface conditions using comprehensive land surface models forced with realistic forcing. These include the Global Soil Wetness Project (http://grads.iges.org/gswp; Dirmeyer et al. 1999), the North America Land Data Assimilation System (NLDAS; K. E. Mitchell et al. 2004), and the Global Land Data Assimilation System (GLDAS; http://ldas.gsfc.nasa.gov; Rodell et al. 2004). These multi-institutional efforts have focused on producing realistic soil moisture and other land surface fields for the recent periods for improving weather and seasonal climate forecasts. Long-term simulations using land surface models have also been done (e.g., Huang et al. 1996; Nijssen et al. 2001a,b, 2003; Dirmeyer and Tan 2001; Maurer et al. 2002; Bowling et al. 2003; Fan et al. 2003; Van den Dool et al. 2003; Fan and Van den Dool 2004; Sheffield et al. 2004; Ngo-Duc et al. 2005). Most of these long-term simulations used the NCEP–NCAR reanalysis data directly as atmospheric forcing. It has been shown that land surface model–simulated fields are sensitive to the large biases in the reanalysis forcing data (Berg et al. 2003). Furthermore, we show here that spurious long-term changes exist in the reanalysis precipitation and surface radiation fields, which make the simulated land surface fields unsuitable for climate change studies.

Many studies have recognized the problems in the reanalysis data. They used observational data either directly or to adjust the reanalysis data. For example, Nijssen et al. (2001b) developed a daily forcing dataset for global land areas for the period of 1979–93, using daily precipitation and daily minimum and maximum temperatures from station observations. Similarly, Maurer et al. (2002) apportioned observed daily precipitation totals evenly over each 3-h period and interpolated temperature through daily maxima and minima to get 3-hourly forcing data for the conterminous United States and portions of Canada and Mexico from 1950 to 2000. Fan and Van den Dool (2004) used the gauge-based monthly Climate Prediction Center (CPC) global land precipitation (Chen et al. 2002) and monthly global reanalysis 2-m air temperature (Kistler et al. 2001) as the driving input fields to derive a global monthly soil moisture dataset for 1948 to 2003. Sheffield et al. (2004) corrected the rain day error in the NCEP–NCAR reanalysis using the monthly precipitation statistics from observations. Ngo-Duc et al. (2005) used the Climate Research Unit (CRU; New et al. 1999, 2000) data to correct the NCEP–NCAR reanalysis precipitation and temperature monthly means and the Surface Radiation Budget (SRB) data produced at the National Aeronautics and Space Administration (NASA) Langley Research Center for a simple bias correction of the reanalysis radiation data.

Hence a central difficulty for performing global land simulations is a lack of multidecadal, high-resolution, realistic atmospheric forcing data for driving land surface models. The forcing data often require subdaily data of precipitation, surface air temperature, specific humidity, wind speed, and downward solar radiation, which are not readily available from observations on a global scale and reanalysis values are flawed. In this paper, we describe a global forcing dataset derived by combining the short-term (synoptic) variations contained in the NCEP–NCAR reanalysis with longer-term variations in monthly time series of observed precipitation, surface air temperature, and other climate records for a 57-yr period (1948–2004) over global land areas. For the observational data, we compare various kinds of products and choose the best available. We then use the forcing data to drive the latest version of the NCAR Community Land Model version 3 (CLM3; Oleson et al. 2004) to simulate the global land surface conditions during 1948–2004, and evaluate the simulations using gauge records of streamflow and available soil moisture data. The deficiencies in the forcing data, the model, and the validation data are

TABLE 1. Datasets used to adjust and validate NCEP reanalysis. All are monthly unless stated otherwise.

Variables	Type and coverage	Resolution	Period	Source and reference
Precipitation	Rain gauge, land	2.5° × 2.5°	1948–2004	CPC; Chen et al. (2002)
Precipitation	Rain gauge and satellite	2.5° × 2.5°	1979–2004	GPCP; Adler et al. (2003)
Precipitation frequency	Global	2° × 2° (seasonal)	1975–97	Dai (2001a,b)
Temperature anomaly	Surface observation, land	5° × 5°	1856–2004	Jones and Moberg (2003)
Temperature climatology	Surface observation, global	1° × 1°	1961–90	New et al. (1999)
Surface solar radiation	Satellite, global	2.5° × 2.5° (3 hourly)	1983–2001	Zhang et al. (2004)
	Station, land	95 stations	1960–90	GEBA; Gilgen et al. (1998)
Cloud cover	Surface observation, land	0.5° × 0.5°	1901–2000	New et al. (2002); T. D. Mitchell et al. (2004)
	Surface observation, global	5° × 4° (seasonal)	1975–2004	Dai et al. (2006)

discussed. We also investigate the effects of precipitation intensity and frequency on the partitioning of precipitation into surface evaporation and runoff. The main purpose of this paper is to document the observation-based forcing dataset that can be used to drive the CLM3 for model development and for simulating past land surface conditions.

In the following, we first describe the forcing dataset in section 2, and then the CLM3 in section 3. An evaluation of the CLM3 simulation is presented in section 4. Section 5 addresses the effects of precipitation frequency on model-simulated fields. A summary and concluding remarks are presented in section 6.

2. Construction of atmospheric forcing data

The atmospheric forcing data for driving the CLM3 include 3-hourly (0000, 0300, 0600 UTC, etc.) precipitation, near-surface air temperature, specific humidity and wind speed, surface air pressure, and downward solar radiation. Since historical records of subdaily precipitation and other fields are unavailable on a global basis, we therefore used the high-frequency variations contained in the NCEP–NCAR reanalysis data, which are 6 hourly (0000, 0600, 1200, 1800 UTC) at T62 (~1.875°) resolution and cover the period from 1948 to present. We used the NCEP–NCAR reanalysis partly because other reanalyses are shorter. The NCEP–Department of Energy (DOE) reanalysis is only for 1979 onward, and while some aspects were improved others got worse. The 40-yr ECMWF Re-Analysis (ERA-40) (September 1957–August 2002) was not available when we started this work and is not as long as the NCEP–NCAR reanalysis; it also has its own problems (e.g., negative $P - E$ over land). We have also created another forcing dataset with ERA-40 adjusted with observations, but it does not make large differences for the CLM3 results reported here. For monthly and longer-term variations, however, we use gridded datasets derived from historical records of station data. Table 1 lists the observational datasets used to create the forcing data. These datasets are regridded to T62 resolution using bilinear interpolation before merging with the reanalysis data.

Near-surface fields of wind speed and air pressure in the reanalysis were updated at least twice daily by radiosonde and satellite observations, and they are used directly here. However, precipitation, surface air temperature, and surface solar radiation are calculated entirely by the atmospheric model used in the reanalysis system (Kalnay et al. 1996) and are not suitable for our purpose, as we show below. It is important to note that surface observations of temperature and precipitation from weather stations were not assimilated into the reanalysis data, even though these observations have provided the basic data for global temperature (e.g., Hansen et al. 2001; Jones and Moberg 2003) and precipitation datasets (e.g., Dai et al. 1997; New et al. 2000; Chen et al. 2002).

Precipitation and clouds have a dominant effect on surface solar radiation, but are notoriously difficult to simulate correctly in atmospheric and climate models (Trenberth et al. 2001a, 2003; Dai and Trenberth 2004). Because of this and the spurious variability resulting from changes and inhomogeneities in the observational data assimilated into the reanalysis, multiyear to multidecadal variations in the reanalysis temperature, precipitation, cloudiness, and surface solar radiation are problematic (Trenberth and Guillemot 1998; Trenberth et al. 2001a,b). Therefore, it is unsuitable to use reanalysis data directly for forcing land surface models in long-term simulations. On the other hand, current weather forecast models capture much of the short-term, synoptic variations at the surface. However, although the reanalysis precipitation diurnal cycle is close to observed-precipitation frequency (Dai 2001b) in summer months for all land areas, it starts too soon after sunrise (~0800 LST) and reaches a plateau versus

a sharp peak in the observations. For winter months, in the extratropics the diurnal cycle is too small in the reanalysis precipitation (not shown). No attempts were made to correct these diurnal biases as any simple corrections would induce physical inconsistencies among the 6-hourly reanalysis data.

a. Precipitation

The NCEP–NCAR reanalysis 6-hourly mean precipitation rates (P_r) at a given grid box were scaled using the observed monthly mean precipitation according to

$$P_{r,\,\mathrm{adj}} = (P_{\mathrm{obs},\,m}/P_{r,\,m})P_r, \tag{1}$$

where $P_{r,\,\mathrm{adj}}$ is the adjusted 4× daily precipitation rate in mm day^{-1}, and $P_{\mathrm{obs},\,m}$ and $P_{r,\,m}$ are, respectively, the observed and reanalysis monthly mean precipitation for month m. A special case (~5% of all cases) occurs when $P_{r,\,m} = 0$ but $P_{\mathrm{obs},\,m} \neq 0$. In this case, a search was employed to find the closest grid cell with at least one nonzero precipitation rate during the month. This grid cell was used to provide $P_{r,\,m}$ and P_r in (1) for the grid cell with zero precipitation rates. If $P_{\mathrm{obs},\,m} = 0$, then $P_{r,\,\mathrm{adj}}$ was set to zero for all time steps within the month.

Chen et al. (2002) created a gridded monthly precipitation dataset for global land from 1948 to present by interpolating rain gauge records from about 5000–16 500 gauges during 1948–97 and about 3500 gauges for more recent years using an optimal interpolation scheme. The undercatch bias associated with topography found in most gridded precipitation datasets (Adam et al. 2006) is considerably reduced in the Chen et al. dataset due to their use of a large network of rain gauges in creating the climatological mean fields (P. Xie 2004, personal communication). For 1997–2004, the Global Precipitation Climatology Project (GPCP) version 2 (v2) dataset (for 1979–2004; Adler et al. 2003) has better gauge coverage than the Chen et al. dataset. There are also other global land precipitation datasets such as those from the CRU (New et al. 2002), the Global Precipitation Climatology Center (GPCC; Beck et al. 2005), and Dai et al. (1997). The CRU dataset uses climatological values to fill many unspecified grid boxes (i.e., the user cannot easily find out which grid box has observations or is filled with climatological values) and its gauge coverage is not better than Chen et al. The GPCC products use total precipitation in gridding (not good for varying station networks), although this is not a big issue for its fixed-station dataset, which uses only about 9000 stations (fewer than Chen et al. for most years). We have compared the various precipitation datasets and found large differences over many areas with sparse gauge coverage such as the Amazon and tropical Africa. Figure 1 compares the time series of annual precipitation averaged over world's major river basins based on five different precipitation products, including the Chen et al., GPCP, CRU, and GPCC fixed-station (VASClimO) and all-station (FullV3) datasets. In general, the Chen et al., CRU, and GPCC FullV3 products are close to each other for most basins, except for the Orinoco and Yenisey. Large spreads exist for the Amazon, Congo, Orinoco, Yenisey, Lena, and Mekong. All the datasets show similar estimates for the Changjiang, Mississippi, and Paraná basins, where good gauge coverage exists. The differences among the precipitation products may result from (a) different gauge coverage especially over tropical Africa and South America, (b) different treatments of wind- and topography-induced undercatch errors by rain gauges (Adam and Lettenmaier 2003; Adam et al. 2006; note only the GPCP v2 has a climatological correction for the wind-induced bias), and (c) differences in gridding methods, which can have considerable effects on the gridded precipitation, especially over sparsely sampled regions (Chen et al. 2002).

Based on our comparisons, here we chose the Chen et al. dataset (for 1948–96), supplemented by the GPCP v2 data for 1997–2004. The GPCP monthly precipitation ($P_{g,\,m}$) for 1997–2004 was adjusted for systematic differences from Chen et al. at each grid box according to

$$P_{\mathrm{obs},\,m} = (P_{c,\,\mathrm{clim}} + 0.01)/(P_{g,\,\mathrm{clim}} + 0.01)(P_{g,\,m}), \tag{2}$$

where $P_{\mathrm{obs},\,m}$ is observational monthly precipitation used for 1997–2004, and $P_{c,\,\mathrm{clim}}$ and $P_{g,\,\mathrm{clim}}$ are the monthly climatology of Chen et al. and GPCP v2 precipitation (mm day^{-1}) over a common period (1986–95), respectively. A precipitation rate of 0.01 mm day^{-1} is added to avoid the few cases of zero in the denominator. Figure 2 shows the difference between the NCEP–NCAR reanalysis and the merged observational precipitation averaged over global and hemispheric land. The reanalysis annual precipitation is about 0.3 mm day^{-1} or 14% higher than the observed for the land areas within 60°S–75°N (Fig. 2a). Furthermore, the reanalysis precipitation apparently has a spurious change around the early 1960s by −0.2 mm day^{-1} in the Northern Hemisphere (Fig. 2b) and around 1974 by +0.4 mm day^{-1} in the Southern Hemisphere (Fig. 2c), while the observations do not show such changes.

The NCEP–NCAR reanalysis 6-hourly precipitation is an average over a 6-h period (centered at 0300, 0900, 1500, and 2100 UTC). We used the 6-hourly mean rates

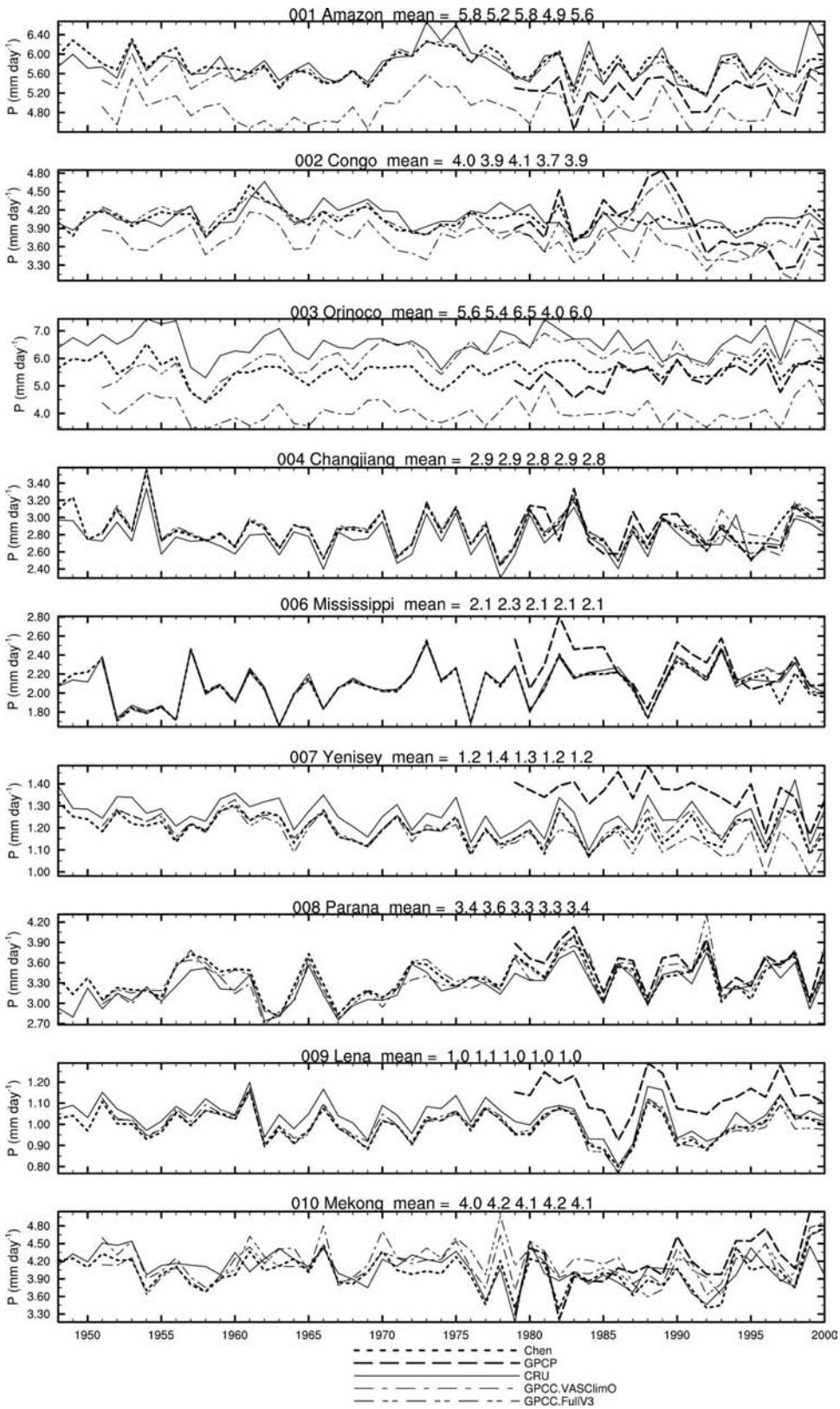

FIG. 1. Time series of annual precipitation averaged over world's major river basins based on five observational datasets: Chen et al. (2002), GPCP, CRU, and GPCC fixed-station (VASClimO) and all-station (FullV3) products. Also shown on the top of each panel are long-term means of these products in the above order.

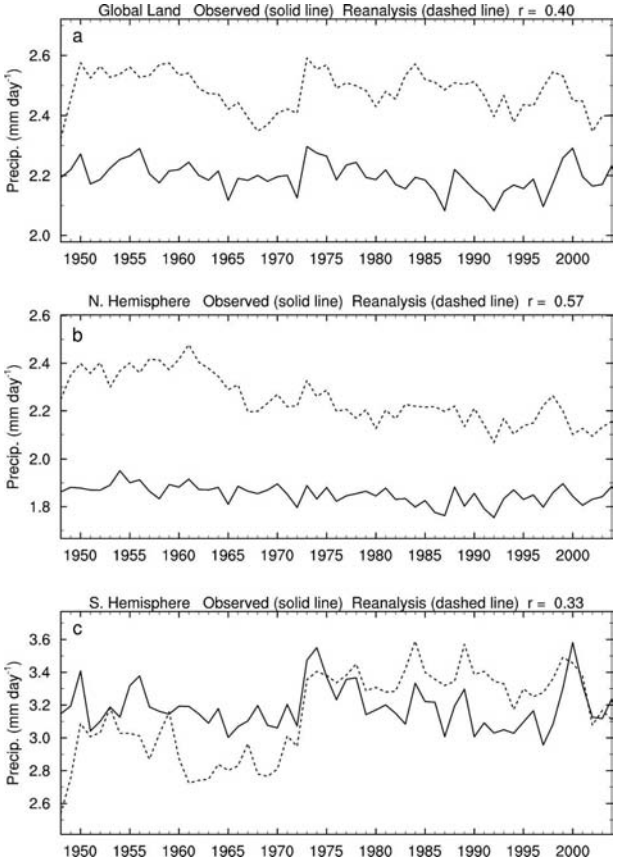

FIG. 2. Time series of annual precipitation averaged over global (60°S–75°N) and hemispheric land areas from rain gauge observations (solid line) and the NCEP–NCAR reanalysis (dashed line). The observations are derived from Chen et al. (2002) for 1948–96 and GPCP v2 (Adler et al. 2003) for 1997–2004 as described in the text.

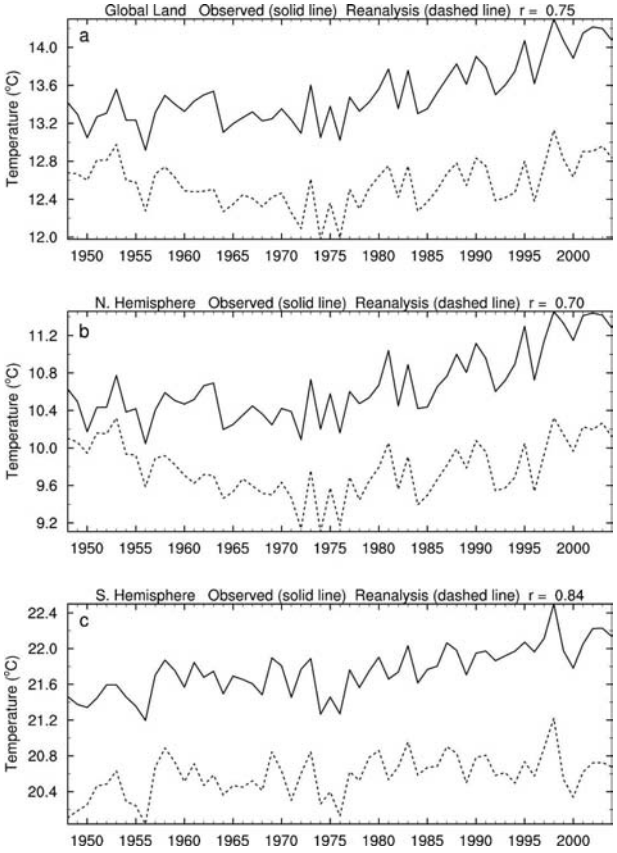

FIG. 3. Time series of annual surface air temperature averaged over global (60°S–75°N) and hemispheric land areas from surface observations (solid line) and the NCEP–NCAR reanalysis (dashed line). The observations are from CRU (Jones and Moberg 2003) with missing values being filled by the reanalysis temperature anomaly added to the CRU 1961–90 climatology.

as the 3-hourly rates for the two 3-h periods within the 6-h period. The diurnal cycle of these 3-hourly precipitation rates is closer to observed-precipitation frequency (Dai 2001b) than linearly interpolated 3-hourly rates.

b. Temperature

The NCEP–NCAR reanalysis 6-hourly surface air temperature at 2-m height (T_r) was adjusted to have the observed monthly value at each grid box according to

$$T_{r,\,\mathrm{adj}} = (T_{\mathrm{obs},\,m}/T_{r,\,m})T_r, \tag{3}$$

where $T_{r,\,\mathrm{adj}}$ is the adjusted temperature, and $T_{\mathrm{obs},\,m}$ and $T_{r,\,m}$ are observational and reanalysis monthly temperatures for month m, respectively. All temperatures are in kelvins.

There are several observational datasets available for monthly surface air temperature over global land, and there are only small differences among them (Folland et al. 2001). Here we used the CRU temperature dataset (Jones and Moberg 2003 and updates). We derived $T_{\mathrm{obs},\,m}$ by adding the monthly temperature anomaly (relative to 1961–90 mean) from Jones and Moberg (2003) to the CRU 1961–90 climatology (New et al. 1999). For certain years, the CRU temperature anomaly dataset contains missing data over small areas (often in tropical Africa, South America, Arctic, and Greenland). We filled the missing data with the NCEP–NCAR reanalysis anomalies relative to the reanalysis 1961–90 mean. After the adjustment, the 6-hourly 2-m temperature (at 0000, 0600, 1200, 1800 UTC) was then linearly interpolated to 3-hourly resolution (at 0130, 0430, 0730 UTC, etc.). Figure 3 shows the difference between the reanalysis and the filled observational temperature. The reanalysis temperature is about 1°C lower than the observed for the mean over global land (Fig. 3a). In the Northern Hemisphere, the reanalysis

temperature has a decreasing trend during 1948–72, which is spurious and not evident in the observations (Fig. 3b). Furthermore, the warming since the late 1970s is larger in the observations than in the NCEP–NCAR reanalysis. This may be partly due to the fact that atmospheric CO_2 and other greenhouse gases were kept constant in the reanalysis (Trenberth 2004).

The differences of annual mean temperature between the NCEP–NCAR reanalysis and the CRU datasets mainly come from the differences in the climatological fields. The large biases over mountainous areas, such as the Rockies, the Andes, and the Tibet Plateau (not shown) are due to several factors including elevation differences of the data grids, snow cover errors in the reanalysis, large uncertainties in the reanalysis land surface model (e.g., in Bowen ratio), errors in reanalysis air flows over mountains (W. Ebisuzaki, NCEP, 2005, personal communication). We emphasize that the 2-m air temperature in the reanalysis is a 6-h forecast and thus depends heavily on the model, and that no surface station observations of air temperature were assimilated into the reanalysis.

c. Surface downward solar radiation

Historical records of surface solar radiation are unavailable over most land areas (Gilgen et al. 1998). Nijssen et al. (2001b) derived daily downward shortwave radiation from daily temperature and precipitation data using an iterative scheme suggested by Thornton and Running (1999). When used in higher temporal resolution, the daily shortwave radiation is disaggregated based on hourly potential solar radiation (Nijssen et al. 2001b; Maurer et al. 2002). Estimates of surface radiation fields based on satellite observations have become available recently (e.g., Zhang et al. 2004); however, they are relatively short in length and often affected by errors in satellite observations of clouds and other atmospheric properties, as discussed below.

Surface downward solar radiation is strongly affected by cloud cover, and it is often modeled using cloudiness data (e.g., Dobson and Smith 1988). The NCEP–NCAR reanalysis downward solar radiation anomaly is highly correlated with the reanalysis total cloud cover anomaly (Fig. 4a). However, the reanalysis cloud cover has a spurious downward trend over global land that is not evident in station data (Fig. 4b). Because of this, we decided to make use of available station data of cloud cover anomaly to adjust the reanalysis monthly surface solar radiation anomaly.

We first performed a linear regression analysis of the monthly anomalies of the downward solar radiation and total cloud cover from the reanalysis at each grid box. We then used this radiation–cloud anomaly relationship and the monthly cloud cover anomaly data derived from station records to compute monthly solar radiation anomalies. We used the CRU_TS_2.02 cloud cover data (New et al. 2002; T. D. Mitchell et al. 2004) from 1948 to 1974; for 1975–2000, we also supplemented the CRU cloud data with our analysis of 3-hourly synoptic observations (Dai et al. 2006); for 2001–2004, the CRU data are unavailable and we used our analysis only. Since surface cloud observations over North America are unreliable after 1994 because of widespread use of automated weather stations (Dai et al. 2006), monthly cloud cover from 124 military stations within the contiguous United States that have continuous human observations were used for January 1995–December 2004 over North America.

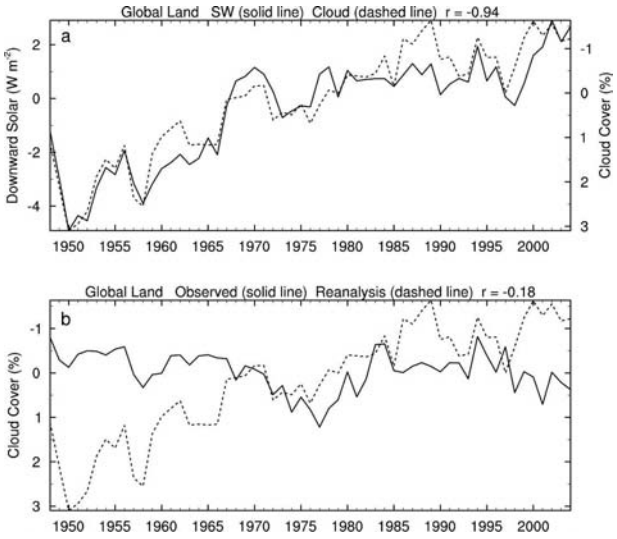

FIG. 4. (a) Anomaly time series of annual surface downward solar radiation (solid line, left ordinate) and total cloud cover (dashed line; increases downward on the right ordinate) from the NCEP–NCAR reanalysis averaged over global (60°S–75°N) land areas. (b) Same as (a) except for surface-observed (solid line) and the NCEP–NCAR reanalysis (dashed line) cloud cover. The cloud observations are derived from the CRU_TS_2.02 dataset (New et al. 2002; T. D. Mitchell et al. 2004) and our analysis of 3-hourly synoptic observations (Dai et al. 2006).

The NCEP–NCAR reanalysis 6-hourly surface downward solar radiation (S_r) was adjusted at each grid box according to

$$S_{r,\,\mathrm{adj}} = (S_{\mathrm{obs},\,m}/S_{r,\,m})S_r, \tag{4}$$

where $S_{\mathrm{obs},\,m}$ is the monthly solar radiation derived using the reanalysis radiation–cloud relationship and observational cloud data (derived by adding the estimated radiation anomaly to the reanalysis mean amount), and $S_{r,\,m}$ is the reanalysis monthly solar radiation. The adjusted solar radiation ($S_{r,\,\mathrm{adj}}$) was evaluated using the

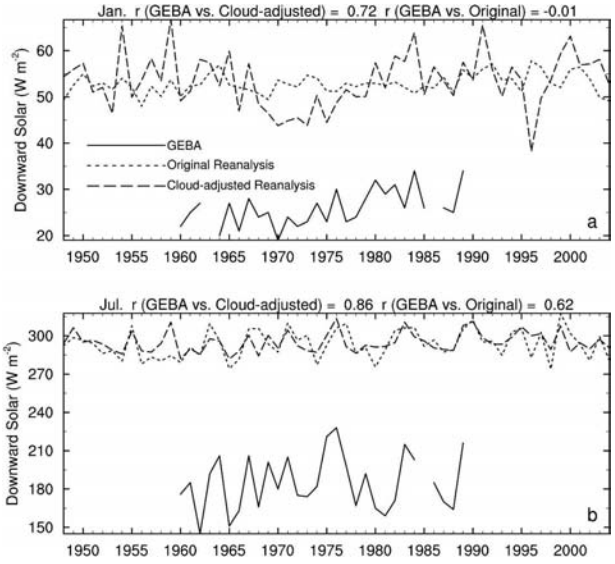

FIG. 5. Comparisons of (a) January and (b) July surface downward solar radiation at a station (52.38°N, 0°) from GEBA surface observations (solid line), the NCEP–NCAR reanalysis (short-dashed line), and cloud-adjusted reanalysis radiation (long-dashed line). Also shown on the top of each panel are (from left to right) correlation coefficients between the observed and cloud-adjusted radiation and between the observed and unadjusted reanalysis radiation.

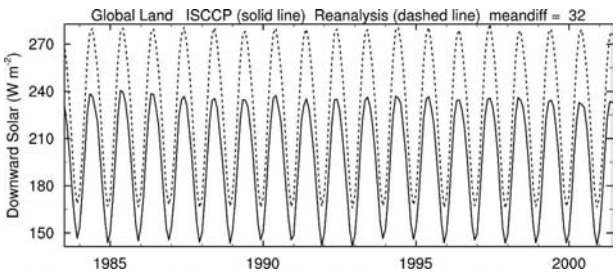

FIG. 6. Comparisons of monthly surface downward solar radiation averaged over global (60°S–75°N) land areas from the ISCCP-based radiation dataset (solid line; from Zhang et al. 2004) and the cloud-adjusted reanalysis radiation (dashed line) from July 1983 to June 2001. Also shown on the top of the panel is the mean difference (cloud-adjusted reanalysis minus ISCCP).

radiation data from the Global Energy Balance Archive (GEBA) database (Gilgen et al. 1998). The GEBA data are available only for a limited number of locations and often with short record length, so we used them only for evaluation purposes. We used 95 stations that have data from 1961 to 1990. We gridded the station data to the T62 Gaussian grid by simply averaging the data within each grid box, and selected the grid boxes with at least 120 months of data over land areas. The cloud-adjusted radiation covaries more closely than the original reanalysis radiation with the GEBA data for most locations; two such examples are shown in Fig. 5. For instance, 40 out of 66 January time series (61%) and 48 out of 70 July time series (69%) have higher correlations with the GEBA data after the adjustment. The large differences of the mean in Fig. 5 result from the biases in the reanalysis mean solar radiation and the fact that the GEBA data are point measurements while the reanalysis data are grid-box averaged values.

The above anomaly adjustment does not affect the mean bias in the reanalysis radiation. To minimize the mean bias, we used the surface downward solar radiation data from July 1983 to June 2001 derived using an atmospheric radiative transfer model and the cloud, surface, and atmospheric properties from the International Satellite Cloud Climatology Project (ISCCP) (Zhang et al. 2004). We did not directly use the ISCCP-based solar radiation data because they have much larger year-to-year variations than the cloud-adjusted reanalysis radiation, which could cause discontinuities of variability with earlier years. Furthermore, the multiyear to decadal variations in the ISCCP-based solar radiation may be affected by spurious changes in the ISCCP cloudiness data associated with changes in satellite orbits and instruments (Dai et al. 2006). The cloud-adjusted reanalysis solar radiation over global land is about 32 W m^{-2} larger than the ISCCP-based estimate for 1983–2001 (Fig. 6). Because the global mean of the ISCCP-based downward solar radiation strongly correlates with the high-quality Baseline Surface Radiation Network (BSRN) measurements for 1992–2001 ($r = 0.98$) with a small bias of 2.0 W m^{-2} (Zhang et al. 2004), we adjusted the mean of the cloud-adjusted reanalysis radiation to the mean of the ISCCP-based radiation at each grid box as described below.

The ISCCP radiation data are approximately 3-h averages, while the NCEP–NCAR reanalysis radiation is 6-h averages. To match the diurnal phase of the two datasets, we first smoothed the ISCCP 3-hourly data to create approximately 6-hourly averages using 1–2–1 weighting. Then we stratified the smoothed data by the 6-h periods (centered at 0300, 0900, 1500, and 2100 UTC) and months, and then averaged them over the 1983–2001 period to derive 18-yr composite monthly radiation fields for each 6-h periods. The same composite maps were derived from the cloud-adjusted reanalysis radiation data. The reanalysis minus ISCCP difference maps of the 18-yr composites for each month and each 6-h period were subtracted from the cloud-adjusted reanalysis radiation for each year of the 1948–2004 period, so that the final adjusted radiation fields have the same mean as the ISCCP radiation data for the 1983–2001 period at each grid box. These cloud- and bias-adjusted 6-hourly radiation data were then

used as 3-hourly data by simply applying the same 6-hourly values over the two 3-h intervals within a 6-h period.

d. Specific humidity, wind speed, and surface pressure

Six-hourly surface specific humidity (q) from the reanalysis was adjusted using the adjusted surface air temperature and original relative humidity from the reanalysis data. Comparisons between the adjusted q and observed q during the 1976–2004 periods (from Dai 2006) showed good agreement. Because surface wind speed and air pressure were calibrated with observations in the reanalysis and because observational datasets for these variables are not readily available, we used the reanalysis data for these two variables directly. These 6-hourly data were linearly interpolated to 3-hourly resolution (at 0130, 0430, 0730 UTC, etc.). Wind speed was taken directly from the 10-m wind components from the reanalysis.

3. Model and simulations

The CLM3 is a comprehensive land surface model designed for use in coupled climate system models. It is described in detail by Dai et al. (2003) and Oleson et al. (2004). In the CLM3, spatial heterogeneity of land surface is represented as a nested subgrid hierarchy in which grid cells are composed of multiple land units, snow/soil columns, and plant functional types (PFTs). Each grid cell can have a different number of land units, each land unit can have a different number of columns, and each column can have multiple PFTs. Biogeophysical processes are simulated for each subgrid land unit, column, and PFT independently and each subgrid land unit maintains its own prognostic variables. The grid-averaged atmospheric forcing is used to force all subgrid units within a grid cell. CLM3-simulated processes include 1) vegetation composition, structure, and phenology; 2) absorption, reflection, and transmittance of solar radiation; 3) absorption and emission of longwave radiation; 4) momentum, sensible heat (ground and canopy), and latent heat (ground evaporation, canopy evaporation, plant transpiration) fluxes; 5) heat transfer in soil and snow including phase changes; 6) canopy hydrology (interception, throughfall, and drip); 7) snow hydrology (snow accumulation and melt, compaction, water transfer between snow layers); 8) soil hydrology (surface runoff, infiltration, subsurface drainage, redistribution of water within the column, which has 10 layers and a fixed depth of 3.43 m); 9) stomatal physiology and photosynthesis; 10) lake temperatures and fluxes; 11) routing of surface runoff to streams and rivers and to oceans; and 12) volatile organic compounds; see Dai et al. (2003) and Oleson et al. (2004) for details of the treatment of these processes and model setups.

Bonan et al. (2002b), Zeng et al. (2002), and Dickinson et al. (2006) examined the CLM3 as part of a coupled climate system model. Global annual averages of temperature and precipitation over land appear to be within the uncertainty of observational datasets but their seasonal cycles seem to be too weak. These studies suggest that the departures from observations appear to be mainly a consequence of deficiencies in the model atmospheric forcing rather than of the land processes, although certain land model deficiencies have been found over various regions, especially over the Amazon (Dickinson et al. 2006).

In this study, we ran the CLM3 in an offline mode forced with the observation-based forcing data described above. Because the water content in deep soil layers takes hundreds of years to spin up and stabilize, we started from the spunup condition of a 480-yr offline simulation forced with recycled 1979–98 NCEP–NCAR reanalysis data (Bonan et al. 2002a). We then ran 220 yr with our 1948–2002 forcing data (recycled after each 55-yr segment) before starting the final 57-yr simulation analyzed here. During the final 57-yr period, the water content in the deepest soil layers vary very slowly and may be considered at equilibrium for our purpose. All of our 55-yr recycled runs and the final 57-yr run were at CLM3's standard resolution of T42 (~2.8°), with the river routing scheme at 0.5° resolution. To test for the effect of resolution, we also ran the CLM3 at 0.5° resolution. For regional and large-scale variations discussed here, the two simulations are comparable, and we therefore only use the T42 simulations in this paper.

4. Evaluation of model simulations

The CLM3-simulated land surface conditions were evaluated using available observational data listed in Table 2. They include historical records or estimates of streamflow and continental freshwater discharge, surface runoff, and soil moisture. It is important to note that differences between the model simulation and validation data may result from errors in the atmospheric forcing data, the land model, and the validation data. Separating and quantifying the individual contributions of these errors are a challenging task. Our goal here is to evaluate the simulated fields for their potential applications in climate change analyses.

a. Effects of the adjustments to the forcing dataset

Figure 7 shows the effects of various adjustments to the forcing data by comparing the seasonal variations of

TABLE 2. Datasets used to validate model simulation. All are monthly unless stated otherwise.

Variables	Type and coverage	Resolution	Period	Source and reference
Streamflow	Station, land		1–100+ year	Dai and Trenberth (2002)
Discharge	Global land	1° × 1°	Climatology	Dai and Trenberth (2002)
Runoff	Global	0.5° × 0.5°		Fekete et al. (2000)
Soil moisture	Station, land		10–21 years	Robock et al. (2000)
	Illinois	19 stations	1981–2001	Hollinger and Isard (1994)
	China	43 stations	1981–91	Robock et al. (2000)
	Mongolia	42 stations	1978–93	Robock et al. (2000)
	Former USSR	50 stations	1972–85	Vinnikov and Yeserkepova (1991)

streamflow rates for world's 10 largest rivers. The simulations were done using three different forcing datasets, that is, the original NCEP–NCAR reanalysis, the reanalysis with precipitation adjustment only, and the fully adjusted forcing data. The streamflow from the unadjusted reanalysis forcing (original) has the largest bias in the annual mean and seasonal amplitude and phase. The precipitation adjustment (PAdj) has the largest improvement (as compared to the temperature and other adjustments), with the amplitude and phase close to the fully adjusted run. The temperature and humidity adjustments (not shown) have only small effects on the river outflow. They decrease the runoff slightly, mainly because the adjustments increase the surface air temperature, which enhances evaporation and thus reduces the runoff. The solar radiation adjustment increases the runoff because the adjustment decreases the surface downward solar radiation, which reduces evaporation and thus enhances the runoff. This makes Changjiang and Brahmaputra much closer to observations, but overestimates the outflow and delays the phase by about one month for the Mississippi (not shown). The fully adjusted (i.e., standard) run shows improved agreement with observations, but there are still noticeable discrepancies, as discussed below.

b. Streamflow

Since the CLM3 routes surface runoff into river channels and simulates streamflow directly, historical records of streamflow from gauge measurements (Dai and Trenberth 2002) provide an independent, rigorous evaluation of land surface hydrology in the CLM3 and the forcings on river-basin scales. Figure 8 compares, on logarithmic scales, the CLM3-simulated long-term-mean downstream river flow rates with observations from nearby gauges (from Dai and Trenberth 2002) for the world's 200 largest rivers. Niger (number 27), Zambeze (number 36), and Nile (number 83) are not included, because their flow rates are unrealistically low in the observational dataset, with runoff efficiency (river flow divided by its basin-averaged precipitation) around 0.03. The simulated and observed streamflow rates are highly correlated ($r = 0.97$ on linear scales and 0.83 on logarithmic scales), with a mean bias (relative to the observation) of -8.9 km^3 yr^{-1}. The large scattering for the smaller rivers in Fig. 8 reflects the fact that streamflow rates for small rivers are more difficult to simulate in percentage terms than for large rivers.

The CLM3 underestimates the outflow from the Amazon River (the upper-right dot in Fig. 8) substantially (by 40%), which is a common bias in many other CLM3 simulations (including runs coupled to an atmospheric model). Dickinson et al. (2006) found that over the Amazon annual evaporation of canopy intercepted water is 34% of rainfall in the CLM3, about twice of what is considered reasonable. Furthermore, 64% of total rainfall over the Amazon is returned to the atmosphere by evapotranspiration, compared with observational estimates of ~50%. Besides these model biases, large uncertainties exist in current estimates of rainfall over the Amazon basin because of sparse observations, as suggested by the large spreads shown in Fig. 1.

Seasonal variations of streamflow for world's 10 largest rivers are simulated reasonably well by the CLM3 (Fig. 7). For example, the CLM3 reproduces the seasonal amplitude and phase for the Amazon River, with a maximum in May and a minimum in November, while the above-mentioned bias exists throughout the year. The mean features of the annual cycle are also captured for the Congo, Orinoco, Changjiang, Brahmaputra, Mississippi, Yenisey, and, to a lesser extent, for the Lena and Mekong. One exception is the Paraná River, which has little seasonal variation in the observations but a considerable annual cycle in the CLM3 simulation. A possible explanation is that streamflow in the Paraná is strongly regulated by large areas of lakes and wetlands in the basin, which smooth out the seasonal variations caused by precipitation (Dai and Trenberth 2002), but these processes have not yet been included in the CLM3. The remarkable match between the simulated and observed peak flow in June for the Yenisey River suggests that the snow model in the CLM3

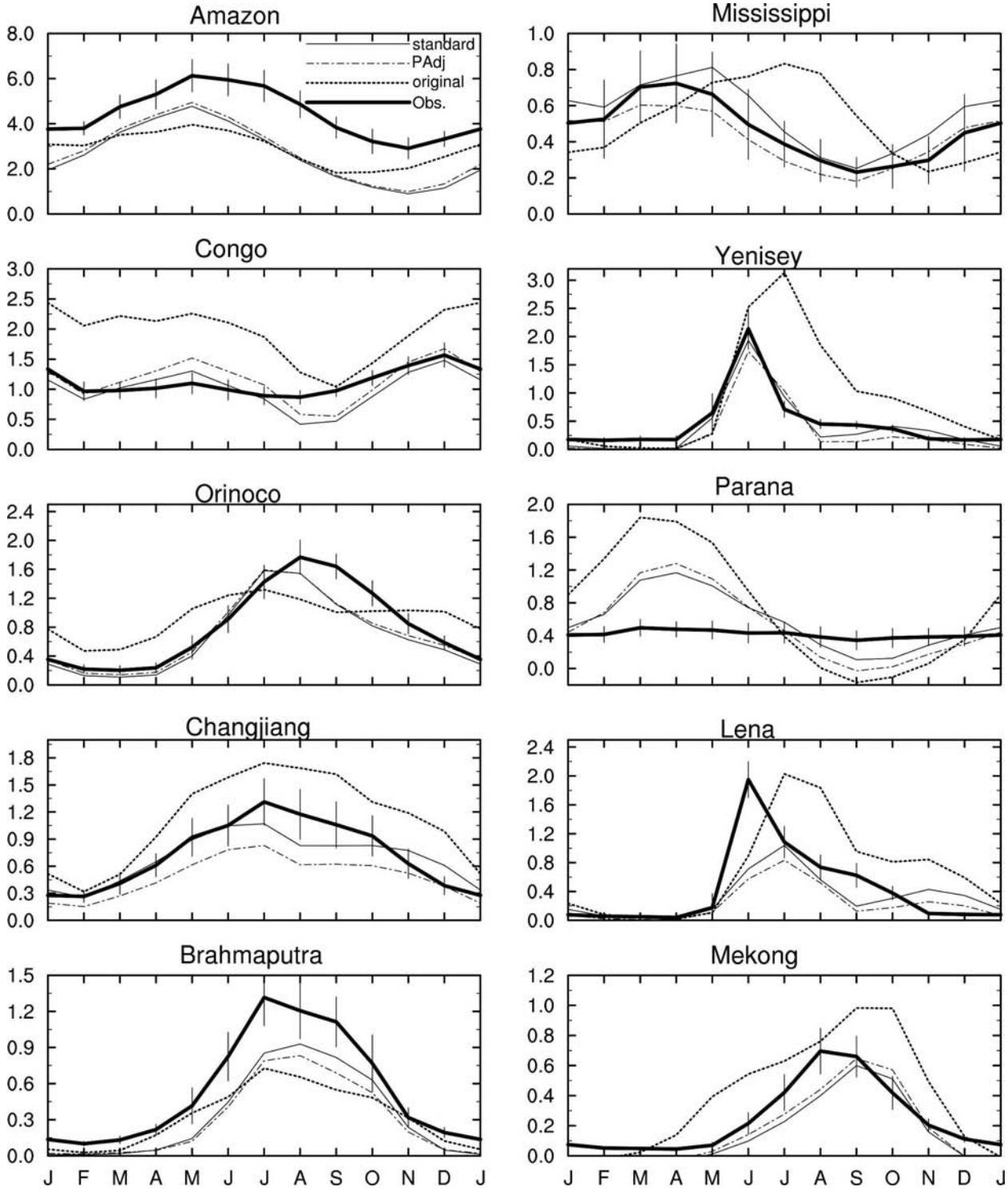

FIG. 7. Mean annual cycle of river outflow rates (10^2 km^3 month^{-1}) for the world's 10 largest rivers simulated by the CLM3 compared to observation (dark line; from Dai and Trenberth 2002). The simulations are based on three different forcing datasets: Original = unadjusted NCEP–NCAR reanalysis; PAdj = the reanalysis with the precipitation adjustment only; and Standard = fully adjusted forcing. The ±1 std dev range of the observed outflow rates for each month is shown by the error bars.

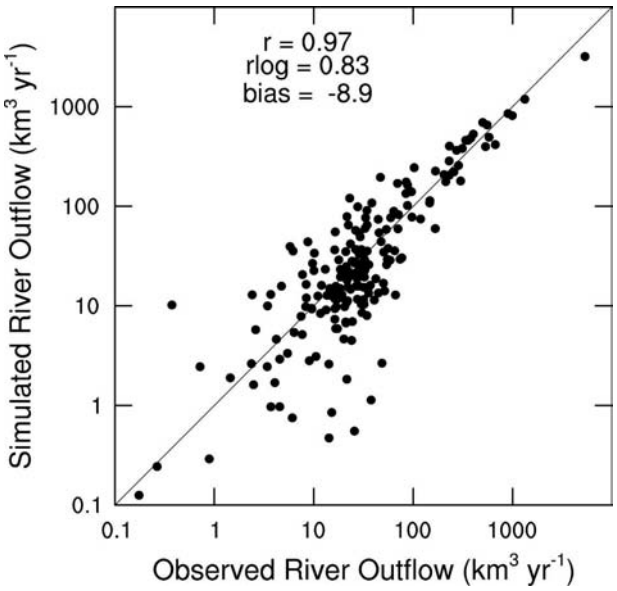

FIG. 8. Scatterplot of observed (from Dai and Trenberth 2002) and CLM3-simulated long-term-mean river outflow rates (km^3 yr^{-1}) for the world's 200 largest rivers. The linear (r) and logarithmic (rlog) correlation coefficients as well as the mean bias (simulated minus observed) are shown.

worked well over that basin, although the simulated spring-to-early summer peak flows are slightly delayed in the Mississippi and Lena Rivers, and is only 50% of the observed peak flow for the Lena River.

To evaluate the variability at time scales longer than one year, we compared time series of water-year (from October-September) mean streamflow from observations and the CLM3 simulation for the world's 10 major rivers, except number 5 Brahmaputra and number 10 Mekong whose streamflow records are too short, plus four smaller rivers that have long records (Fig. 9). To emphasize the variability, we use different scales for the observed and CLM3 curves because mean biases exist for many rivers (as shown in Figs. 7 and 8). The simulated and observed streamflow covary closely on both interannual and longer time scales for all of the 12 rivers except the Yenisey and Lena Rivers. Large decadal variations are evident in both observed and simulated flows for many of the rivers. For example, the Congo River had relatively high streamflow in the 1960s when low streamflow occurred in the Paraná River. In the much smaller Susquehanna basin in the northeast United States, relatively low flows occurred in the 1960s followed by high flows in the 1970s. Streamflow has increased since the 1950s in the Mississippi and Paraná Rivers due to increased precipitation in these regions (Dai et al. 1997).

The correlation between observed and simulated streamflow for the two Russian rivers (Yenisey and Lena) is relatively low (Fig. 9). For Lena, the correlation increases to 0.66 when the calendar year instead of the water year is used. For Yenisey, observations suggest an upward trend since the 1960s, which is not evident in the CLM3 simulation (Fig. 9). Records from the next upstream gauge at P. Tunguska along the Yenisey River covary ($r = 0.67$) with the farthest downstream flow from a gauge at Igarka (shown in Fig. 9), suggesting that the Yenisey streamflow data are reliable. The discrepancy between precipitation and streamflow over major Russian rivers has been noticed before (e.g., Berezovskaya et al. 2004). Errors in precipitation data due to sparse rain gauges (Chen et al. 2002) and undercatch (Adam and Lettenmaier 2003) over Russia likely contributed to the relatively low correlation and large negative biases between the observed and CLM3-simulated streamflow. Another possibility is that recent warming over Eurasia may have increased the thawing of permafrost (which changes runoff but is not simulated in the CLM3) and thus contributed to the streamflow increases. However, McClelland et al. (2004) concluded that permafrost thawing is unlikely to be a major contributor to the observed streamflow increases in the Yenisey and other Russian rivers. Warming-induced changes in snowmelt should mostly alter the annual cycle, with small effects on the annual mean flow. Withdrawal of stream water for industrial and agricultural use during recent decades should decrease the river flow while large dams should mostly alter its annual cycle (Yang et al. 2004); they cannot explain the upward trend in Yenisey's flow rates since the 1960s, as pointed out by Dai et al. (2004).

c. *Continental freshwater discharge*

The second evaluation is against the observation-based estimates of continental freshwater discharge into the ocean basins at each latitude, which is important for freshwater budgets within the oceans and for regional (e.g., Nakamura 1996) and global thermohaline (e.g., Dai et al. 2005) ocean circulations through changes in density. To estimate continental discharge, a river transport model that routes terrestrial runoff into correct river mouths is needed. Since time series of continental discharge into the individual and global oceans cannot be reliably estimated from incomplete gauge records of streamflow alone (Dai and Trenberth 2002), the CLM3 simulated river outflow can supplement the gauge data if they are evaluated to be reasonable.

Figure 10 shows the (smoothed) latitudinal distribution of long-term-mean annual continental freshwater

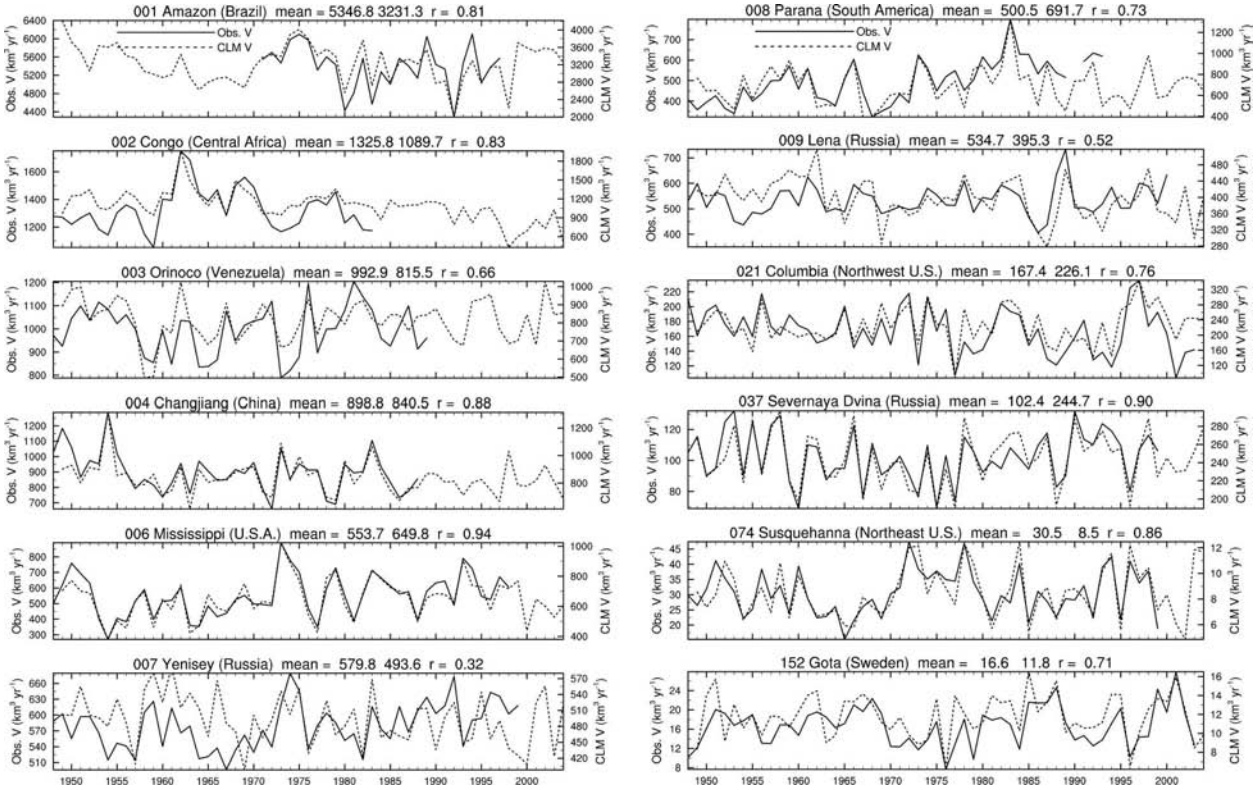

FIG. 9. CLM3-simulated (dashed) and the observed (solid) water-year (October–September) river outflow rates for world's 10 largest rivers (except No. 5 Brahmaputra and No. 10 Mekong whose records are too short), and four smaller rivers that have long records. Also shown on the top of each panel are (from left to right) long-term means of the observed and CLM3-simulated rates, and the correlation coefficient (r) between the two curves.

discharge into the global oceans. The CLM3 simulated discharge reproduces the peak outflows from the world's largest rivers, although the model underestimates the discharge within 8°S–22°N. This is especially true for the Amazon, with 0.21 Sv (1 Sv $\equiv 10^6$ m^3 s^{-1}) in the observations and only 0.13 Sv in the CLM3, consistent with the large negative bias in Amazon streamflow identified in section 4a. This is also the case for the Atlantic Ocean because the Amazon accounts for more than one-third of the total discharge to the Atlantic. In section 5, we reevaluate the continental discharge after we alleviate the evapotranspiration bias for the Amazon basin. For the Pacific Ocean, the difference in the accumulated discharge between the CLM3 and the 921-river-based estimate increases from south of 30°N and reaches about 0.5 Sv. For the Indian Ocean, the CLM3 slightly underestimates the 921-river-based accumulated discharge north of 20°N, while overestimates it south of 20°N (not shown). Note that the CLM3-simulated discharge south of 60°S (Fig. 10) should be interpreted cautiously as the forcing data, especially precipitation, are unreliable at those latitudes. In summary, despite the biases associated with errors in pre-

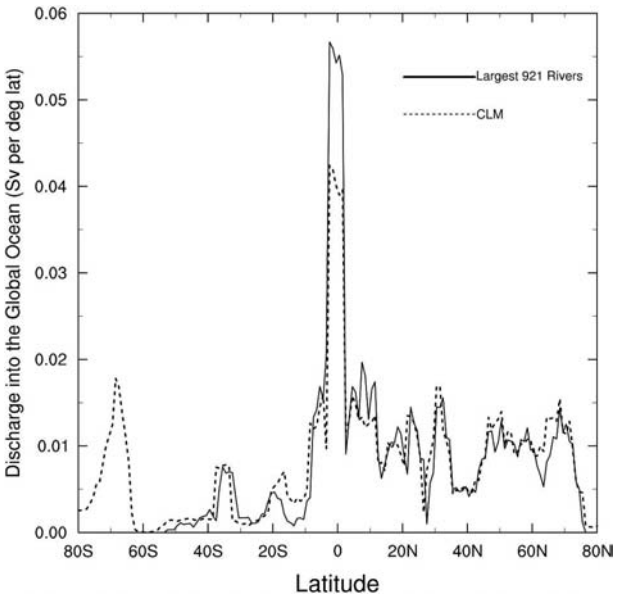

FIG. 10. Long-term-mean annual freshwater discharge (Sv) into the global oceans smoothed using a 5° lat running mean from observation-based estimates (solid line; from Dai and Trenberth 2002) and the standard CLM3 simulation (dashed line).

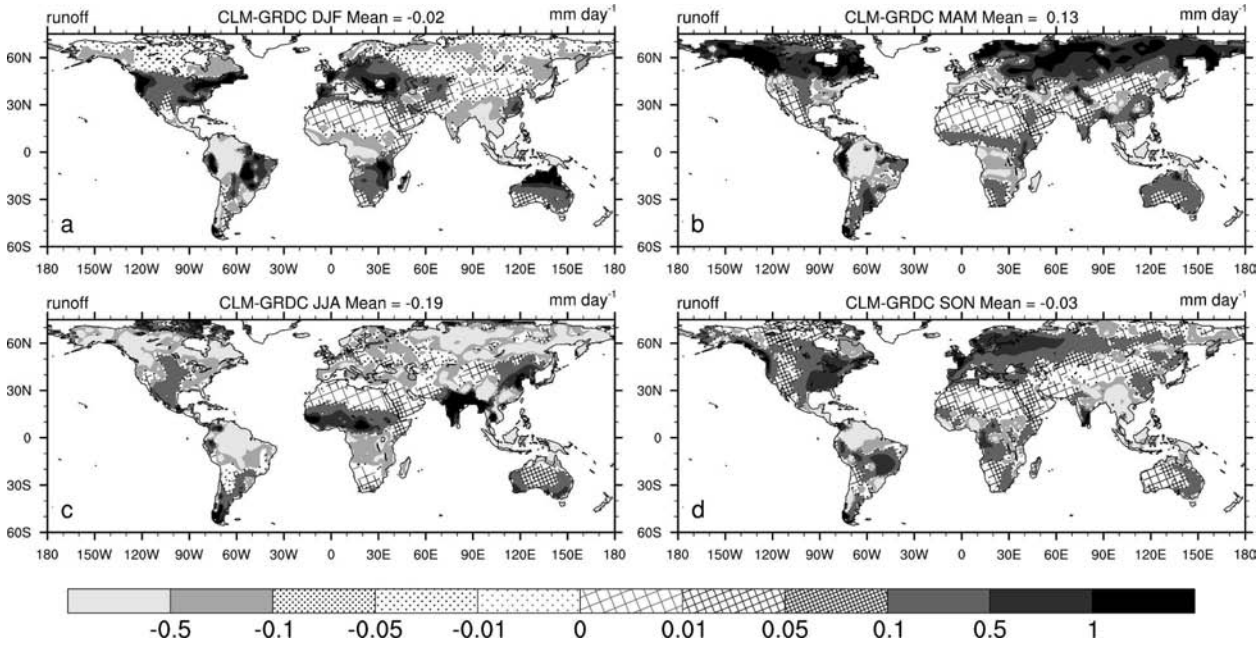

FIG. 11. Long-term-mean differences of total runoff (mm day^{-1}) from the CLM3 simulation and observation-based estimates (from Fekete et al. 2000, 2002) for the four seasons (a) December–February, (b) March–May, (c) June–August, and (d) September–November.

cipitation and other forcing data and the inadequate resolution to resolve complex terrain in the river routing scheme, the CLM3-simulated continental discharge is reasonable.

d. Runoff

Next we evaluate the CLM3-simulated total runoff. The evaluation data we used are from Fekete et al. (2000, 2002), who used long-term-mean streamflow data from 663 gauge stations to calibrate the global runoff fields calculated from a water balance model, resulting in a monthly climatology (mostly for the 1950–90 period) of runoff at 0.5° resolution. Although not pure observational data, their runoff fields probably represent one of the best estimates of global runoff currently available.

The CLM3-simulated mean annual total (including surface and subsurface) runoff averaged over global land is 0.74 mm day^{-1}, which is 0.03 mm day^{-1} or 4% lower than the Fekete climatology (0.77 mm day^{-1}). This underestimation is consistent with the undercatch of precipitation by rain gauges (Adam and Lettenmaier 2003) and by gridded precipitation datasets due to orographic effects (Adam et al. 2006). It may also result from other biases in the forcing data, such as the rain-day frequency biases in the NCEP–NCAR reanalysis (Cullather et al. 2000; Serreze and Hurst 2000; Sheffield et al. 2004), and the biases in the number of above-freezing days that force snowmelt.

The seasonal runoff difference maps (Fig. 11), however, suggest that there are other processes (e.g., related to land water storage) contributing to the CLM3 runoff biases. Undercatch biases of solid precipitation by rain gauges in boreal spring in northern mid- and high latitudes cannot explain the large positive bias (~0.5–1.5 mm day^{-1}or 100%–200% of Fekete climatology) in the simulated runoff in these regions, where runoff also has large negative biases (~−0.2 to −1.0 mm day^{-1} or −50% to −100%) in summer. The reasons for the overestimation of runoff in northern mid- and high latitudes in spring and underestimation in summer may be linked. If spring melt (and therefore runoff) is overestimated, then summer soil moisture and melt (and runoff) will be underestimated. The reason for the overestimation in spring may be due to inaccurate snow physics in the model and/or how the model differentiates between rain and snow. Another factor is that the model is tuned to high-frequency, low-intensity precipitation, which also causes underestimation of runoff in the summer.

Another feature is the negative bias (~−0.3 to −1.5 mm day^{-1} or −20% to −30%) in all seasons over tropical land areas, especially in the Amazon basin, which significantly reduces the streamflow in the Amazon River. These seasonal biases are very large in percent-

age terms. As pointed out in section 4b, this suggests too much evapotranspiration over the Amazon, consistent with the findings of Dickinson et al. (2006).

Figure 12 shows the partial correlation, in which the effects of other variables are removed, of the simulated annual runoff with three forcing variables: annual precipitation, air temperature, and downward solar radiation. It clearly shows that runoff is determined predominantly by precipitation, with a global land mean partial correlation coefficient of 0.70 and thus contributing about 49% to the total variance of runoff. Surface temperature and solar radiation are negatively correlated with runoff over most land areas as surface evaporation generally increases with these two variables. However, seasonally, these variables clearly play an important role in snowmelt and resulting runoff.

e. Soil moisture

There are only sparse records of soil moisture (Robock et al. 2000) that can be used to evaluate the CLM3 simulation. The soil moisture stations (see Table 2 and Robock et al. 2000) were averaged over regions defined by latitudes and longitudes to facilitate comparisons with the gridded model output because soil moisture has large variability at point and grid scales (Robock et al. 1998; Entin et al. 1999). A few very close stations were averaged first and then combined with other stations to obtain the arithmetic mean for the region (Dai et al. 2004).

For Illinois, the simulated monthly soil moisture content follows closely with the observed, with a correlation of 0.73 (0.87 with the annual cycle included) (Fig. 13a). The mean annual cycle (Fig. 13b) and its monthly tendency (Fig. 13c) are also well simulated by the CLM3, although the model underestimates the mean soil moisture content by about 60 mm or about 20%, mainly in southern Illinois. The simulated monthly soil moisture content anomaly over the former USSR regions 1 and 2 (Figs. 14a,b) and east and south China (Figs. 14c,d) also covary with the observation, but with positive biases, especially in the two former USSR regions and south China. Significant correlations with limited soil moisture data are also found over Mongolia, although substantial mean biases exist (not shown).

Partial correlations of the CLM3-simulated annual soil moisture content with three forcing variables (Fig. 15) suggest that soil moisture content is positively affected by precipitation, but negatively correlated with surface temperature and solar radiation over most land areas, consistent with the notion that precipitation increases soil wetness while higher surface temperatures and solar heating increase evaporation.

5. Effects of precipitation frequency on evaporation and runoff

Because it rains only a fraction of the time, precipitation frequency and intensity are two other characteristics that can be as important as the amount in partitioning rainfall into storage and runoff (Trenberth et al. 2003). For example, a severe thunderstorm may create a lot of surface runoff or even flash floods, but still leave the subsurface soil dry. In contrast, hours of light, stratiform rain can moisten the soil thoroughly with little runoff.

A common problem in the offline and coupled CLM3 simulations is the systematic underestimate of runoff fields in the Tropics (the Amazon basin, tropical Africa, and Indonesia region) (Fig. 11). This implies positive biases in surface evapotranspiration. A possible reason for these biases is that 3-h mean precipitation rates were applied to all time steps, whereas in reality precipitation occurs only part of the time (Dai 2001a). To minimize this problem, we used seasonally and diurnally varying precipitation frequency maps from Dai (2001a,b) to modify the 3-hourly mean precipitation rates, so that on average precipitation has a realistic combination of frequency and intensity, in addition to the correct amount. For example, with a time step of 20 min with the CLM3, if the precipitation frequency is 11% (i.e., 1/9) at a grid box, then the 3-h total precipitation is allowed to occur only in one of the nine 20-min time steps within the 3-h time period at a rate of 9 times the 3-h mean rate. It should be noticed that the frequency adjustment is imperfect because it does not change the reanalysis daily precipitation frequency and intensity.

Figure 16 shows that the largest differences in land evaporation and runoff between the frequency-adjusted and standard (i.e., forced with 3-hourly mean precipitation rates) runs occur in the Tropics, where evaporation decreases and runoff increases. This is especially true in the Amazon basin, where runoff increases by 0.5–1.5 mm day^{-1} and total evaporation decreases by a similar amount. In contrast, the difference is small at middle and high latitudes (Fig. 16), where precipitation occurs more frequently than in the Tropics (Dai 2001a). However, the precipitation frequency adjustment does increase annual runoff in northern midlatitudes mostly by increasing the runoff (i.e., reducing the negative bias) in summer. It has only small influences in spring and autumn, and little effect in winter. This is because nondrizzle precipitation at middle and high latitudes is most frequent in December–February (DJF). This high-frequency band at northern latitudes disappears in June–August (JJA) and is weaker

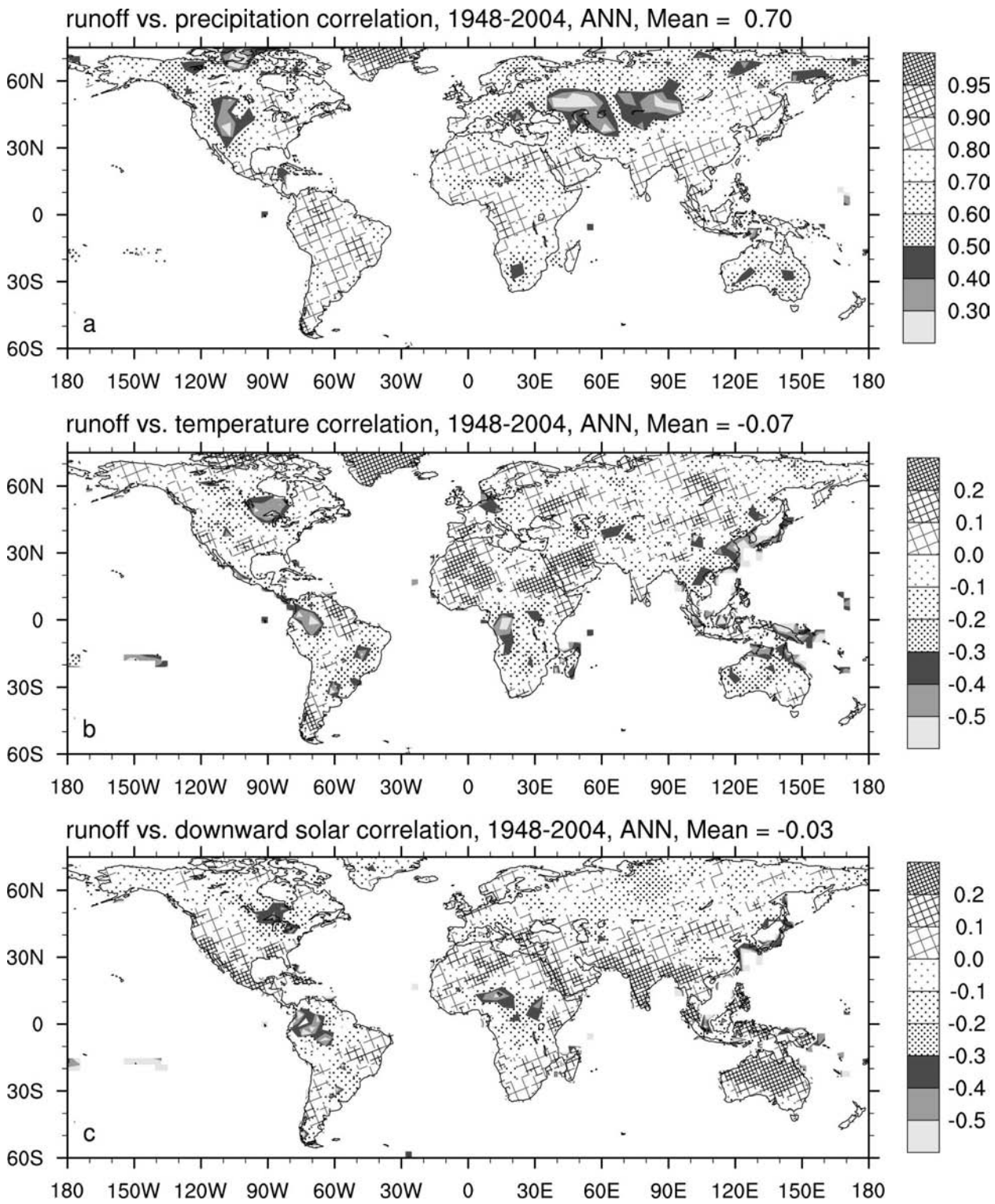

FIG. 12. Maps of partial correlation coefficients between the CLM3-simulated annual total runoff and the input annual forcing: (a) precipitation, (b) temperature, and (c) surface downward solar radiation.

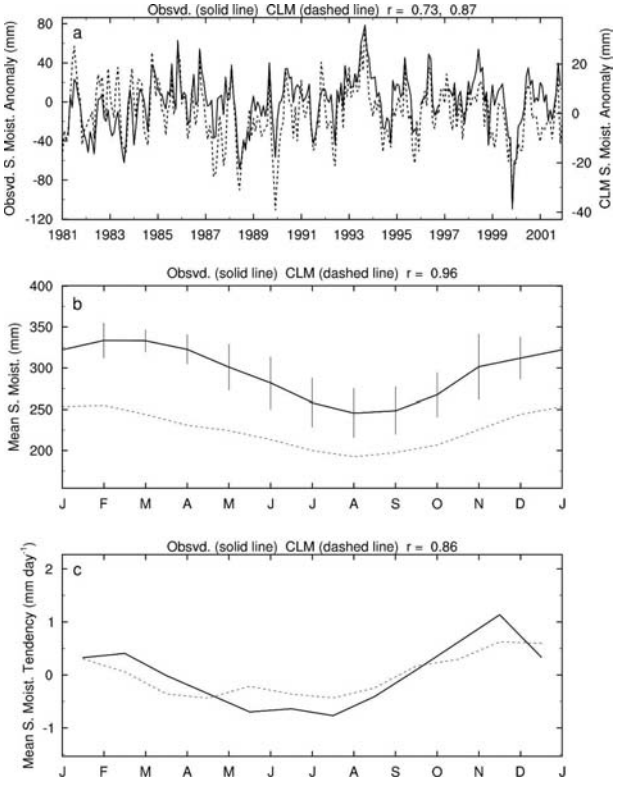

FIG. 13. Observed soil moisture content within the top 0.9-m depth (solid) compared with the CLM3 simulated values (dashed) over Illinois for the same period: (a) monthly anomaly time series; (b) mean annual cycle (with the ±1 std dev error bars); and (c) mean soil moisture tendency for each month. Also shown on the top of each panel is the correlation coefficient (r) between the two curves; in (a) the second value is the correlation coefficient including the annual cycle.

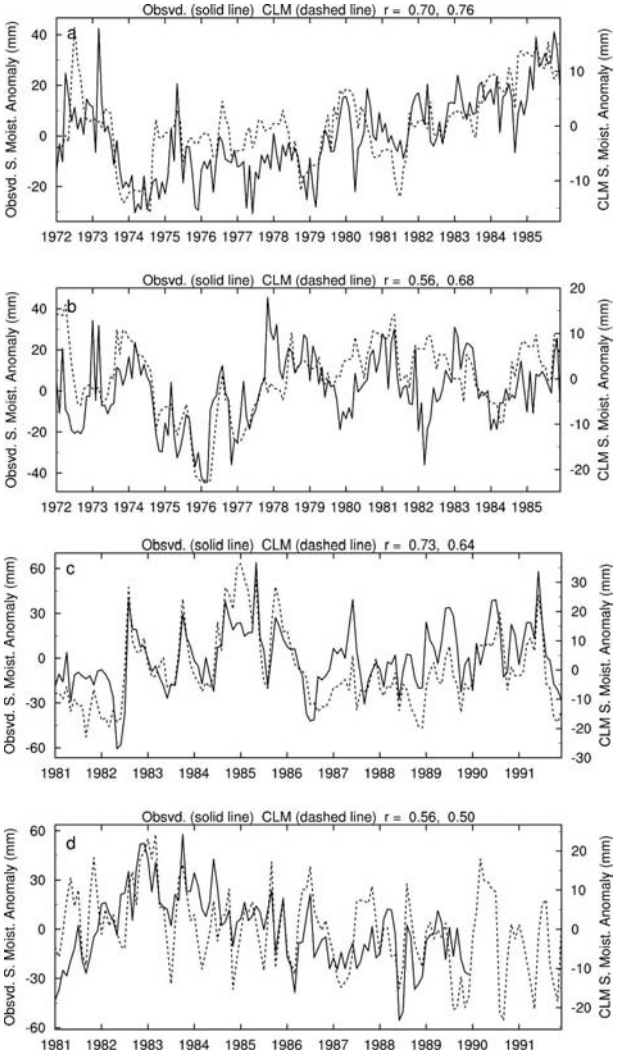

FIG. 14. Monthly anomaly time series of observed soil moisture content within the top 1-m depth (solid) averaged over (a) the former USSR region 1 (50°–55°N, 70°–100°E), (b) region 2 (47.5°–55°N, 45°–60°E), (c) east China (32.5°–35.0°N, 110°–120°E), and (d) south China (22.5°–25.0°N, 102.5°–110.0°E) compared with the CLM3-simulated values (dashed). Also shown on the top of each panel are (from left to right) the correlation coefficients (r) between the two anomaly curves and monthly time series with the annual cycle.

in March–May (MAM) and September–November (SON) as the synoptic activity weakens (Dai 2001a).

For the 200 largest rivers, the mean bias of annual streamflow is 6.4 $km^3\ yr^{-1}$ and the correlation is 0.98 in the frequency-adjusted run (Fig. 17), which are improvements over $-8.9\ km^3\ yr^{-1}$ and 0.97, respectively, in the standard run. In particular, the streamflow rate is greatly improved for the Amazon River, with the long-term mean increased by 31% to 4248 $km^3\ yr^{-1}$. Although it is still lower than the station data, the negative bias is half of that in the standard run. As a result, the accumulated discharge to the global ocean (Fig. 18) is much closer to the 921-river-based estimate than the standard run, especially in the Tropics (Fig. 10). The most significant change is for the Atlantic Ocean because of the improved Amazon outflow.

While the adjustment of the precipitation rates using observed-precipitation frequency maps should result in more realistic precipitation forcing, the CLM3 may have been tuned to unrealistic high frequency and low intensity of precipitation from atmospheric general circulation models (Dai and Trenberth 2004). This may explain why the simulated streamflow from the Congo and Paraná is too high in the frequency-adjusted run (not shown). Therefore, we presented results from the standard run in most of our analyses.

6. Summary and concluding remarks

To provide a realistic atmospheric forcing dataset for land model development and for long-term simulations

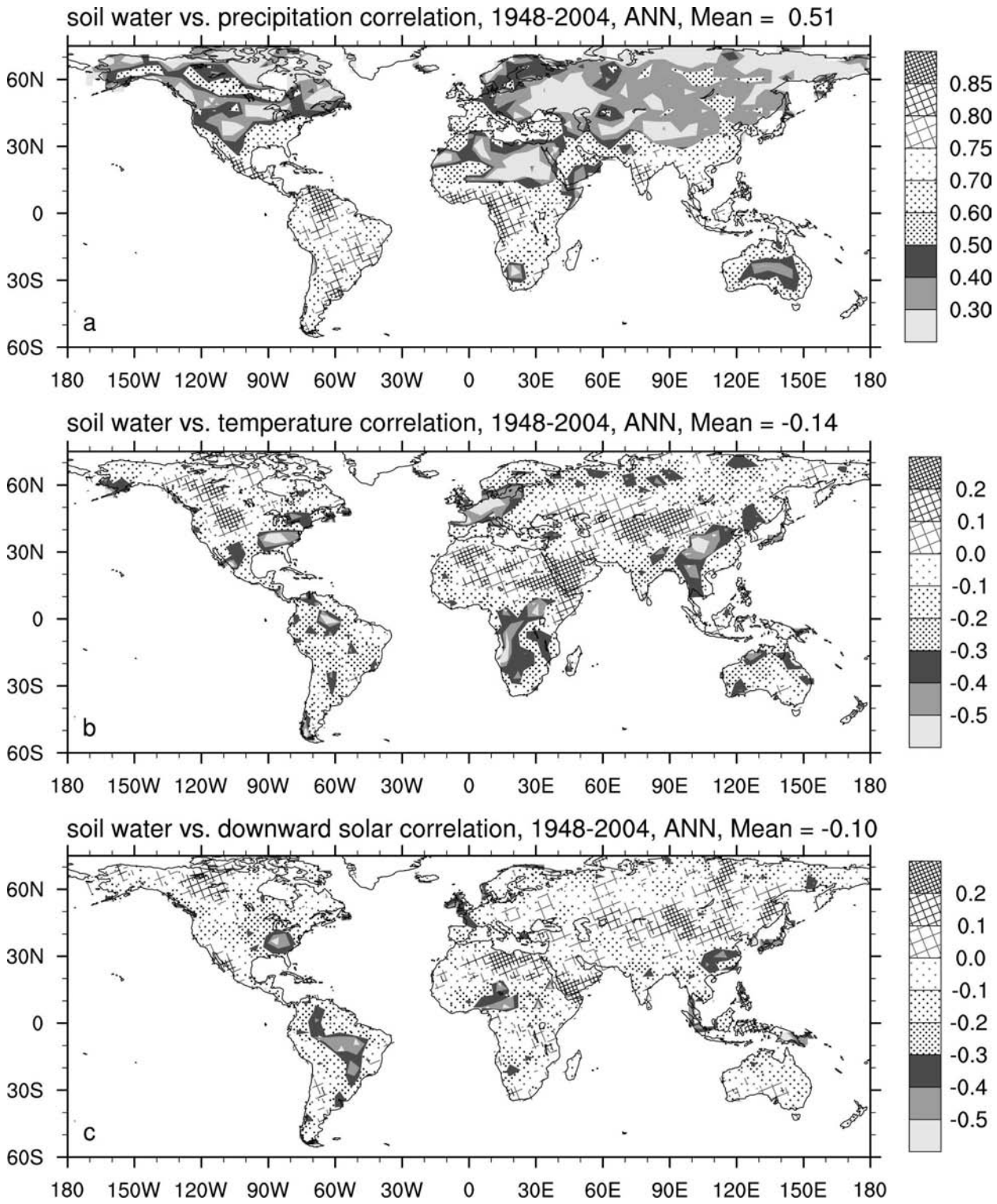

FIG. 15. Maps of partial correlation coefficients between the CLM-simulated annual soil moisture content within the top 1-m depth and the input annual forcing: (a) precipitation, (b) temperature, and (c) surface downward solar radiation.

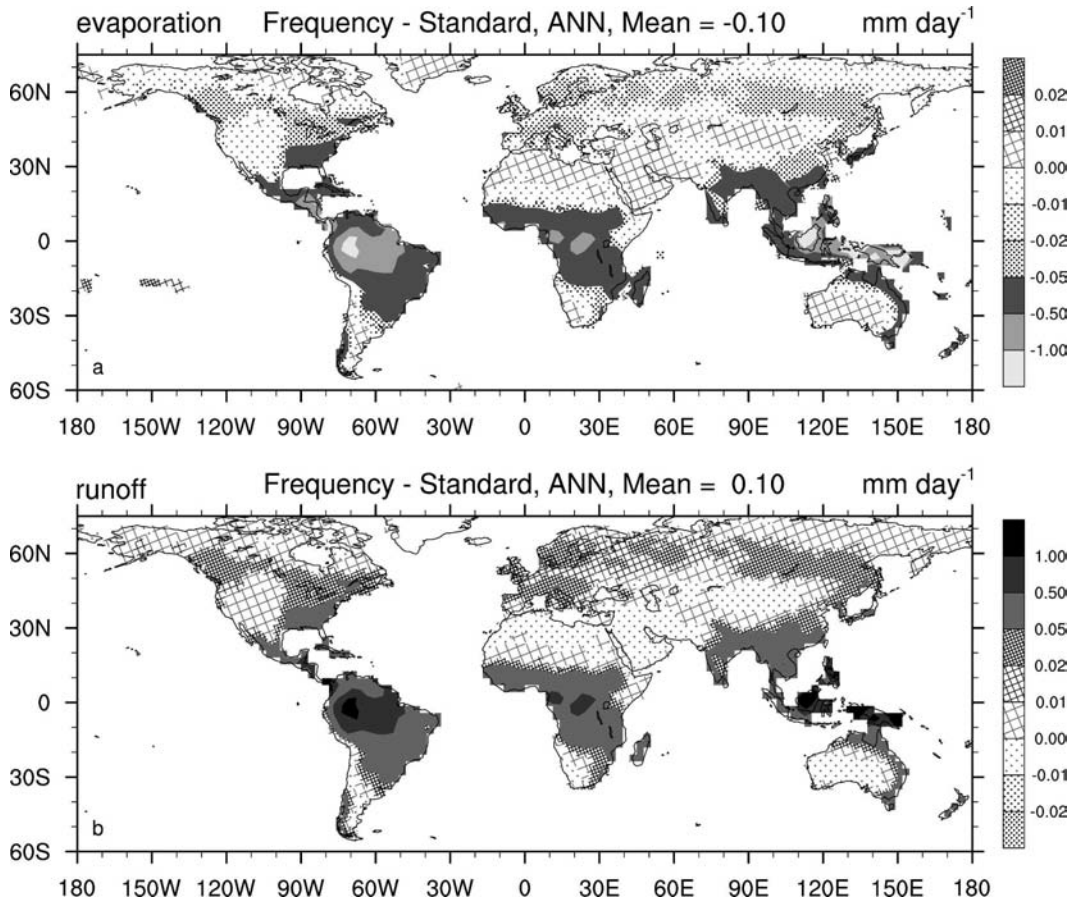

FIG. 16. (a) Total evaporation and (b) total runoff differences of the CLM3 simulation with precipitation frequency minus the standard CLM3 simulation for the 1948–2004 annual mean.

of historical land surface conditions, we have produced a global, 3-hourly forcing dataset for driving the CLM3 from 1948 to 2004. The simulations were evaluated with available data of streamflow, continental freshwater discharge, surface runoff, and soil moisture.

The forcing dataset covers the global land areas at 3-hourly and T62 (~1.875°) resolution from 1948 to 2004. It includes precipitation, surface air temperature, downward solar radiation, specific humidity, wind speed, and air pressure. To correct the spurious long-term changes and biases in the NCEP–NCAR reanalysis precipitation, surface air temperature, and solar radiation fields, we combined the intramonthly variations from the NCEP–NCAR 6-hourly reanalysis with monthly time series derived from station records of temperature and precipitation. Surface downward solar radiation from the reanalysis was first adjusted for variations and trends using monthly station records of cloud cover anomalies and then for mean biases using satellite observations of recent decades. Six-hourly surface specific humidity from the reanalysis was adjusted using the adjusted surface air temperature and original relative humidity from the reanalysis data. Surface wind speed and air pressure were interpolated directly from the reanalysis data. A series of CLM3 runs were conducted to assess the effects of the adjustments to the NCEP–NCAR reanalysis data. The precipitation adjustment was found to have the largest improvement, while the temperature and radiation adjustments have only small effects.

When forced by this dataset, the CLM3 reproduces many aspects of the long-term mean, annual cycle, interannual and decadal variations, and trends of streamflow for many large rivers (e.g., the Orinoco, Changjiang, Mississippi, etc.), although substantial biases exist. The simulated long-term-mean freshwater discharge into the global and individual oceans is comparable to 921 river-based observational estimates. Observed soil moisture variations over Illinois and parts of Eurasia are generally simulated well, with the dominant influence coming from precipitation. It is also shown that unrealistically low intensity and high frequency of

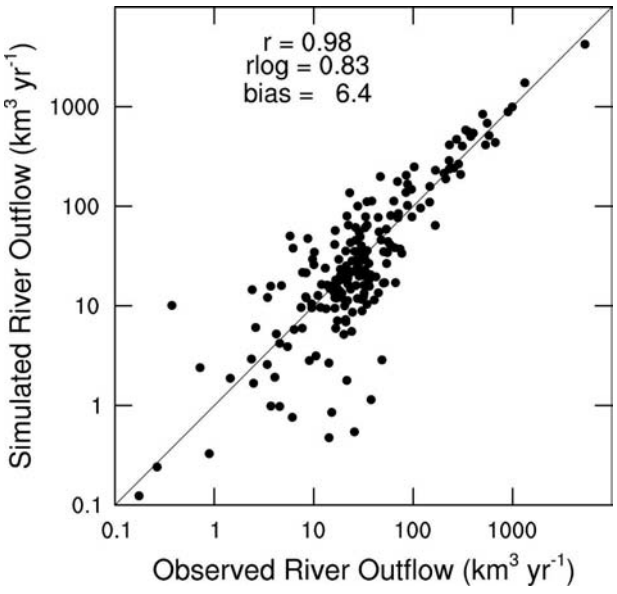

FIG. 17. Scatterplot of observed and CLM3-simulated (with realistic precipitation frequency) long-term-mean annual river outflow rates ($km^3\ yr^{-1}$) for the world's 200 largest rivers. The linear (r) and logarithmic (rlog) correlation coefficients as well as the mean bias (simulated minus observed) are shown.

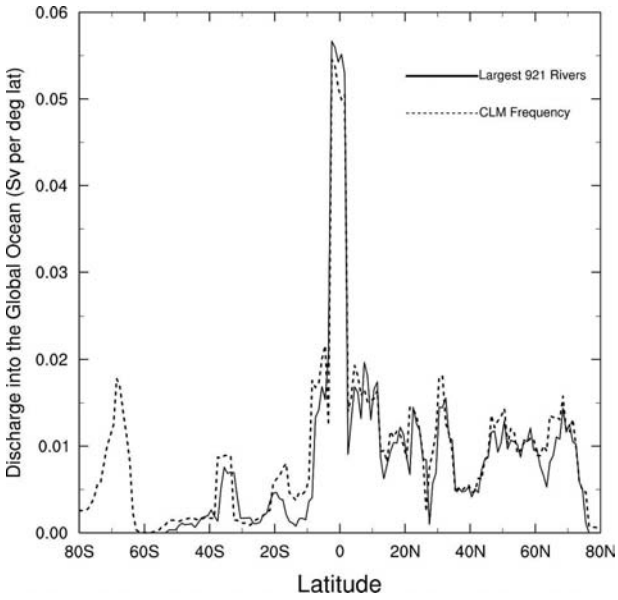

FIG. 18. Long-term-mean annual freshwater discharge into the global oceans smoothed using a 5° lat running mean from observation-based estimates (solid line; from Dai and Trenberth 2002) and the CLM3 simulation with realistic precipitation frequency (dashed line).

precipitation, as in most model-simulated precipitation or observed time-averaged fields, result in too much evaporation and too little runoff, which leads to lower than observed river flows. This problem can be reduced by adjusting the precipitation rates using observed-precipitation frequency maps.

The forcing dataset created here likely contains considerable errors. For example, we used the rain-gauge-based estimates of land precipitation from Chen et al. (2002) and the GPCP v2 (Adler et al. 2003, for 1997–2004 only). Chen et al. precipitation is not corrected for wind-induced undercatch biases, which are most pronounced for solid precipitation and may be as high as 12% for annual precipitation over global land (Adam and Lettenmaier 2003). Neither precipitation product is corrected for the topography-related underestimate bias over mountainous regions that could be 10% or more locally (Adam et al. 2006), although this is likely minimized by the large network of rain gauges used by Chen et al. to create their monthly climatology. The correction of the undercatch biases due to winds, wetting, and evaporation requires additional historical data such as surface wind speed, precipitation phase (liquid versus solid), and rain gauge types (Legates et al. 2005), which are not readily available on a global scale. The precipitation biases, as well as the human influences on natural streamflow, such as withdrawal of stream water and dams and reservoirs, hamper our ability to precisely evaluate the CLM3 simulations using historical records of streamflow, although our results suggest that the CLM3 evaporates too much over tropical rain forests, especially in the Amazon.

The adjustment of the solar radiation using the often-incomplete cloudiness data also likely contains large uncertainties as historical records of cloud cover contain large uncertainties and have sparse sampling over many regions such as Africa and South America. While the adjustment of the precipitation rates using observed-precipitation frequency maps should result in more realistic precipitation forcing, this adjustment is imperfect as it does not correct the bias in the reanalysis rain-day frequency. Furthermore, many land surface models such as the CLM3 may have been tuned to unrealistically high frequency and low intensity of precipitation, as these land models are usually coupled to atmospheric general circulation models whose precipitation fields often contain these biases (Dai and Trenberth 2004).

These uncertainties and biases in the forcing dataset suggest that the CLM3 simulations of land surface conditions likely contain biases and comparisons with streamflow and other observations will be imperfect. Nevertheless, running land surface models with our forcing data provides a better framework for testing model physics and parameterizations than using reanalysis or atmospheric model data, as the latter often

contain much larger biases in precipitation, temperature, and other fields. Our results show that the CLM3 historical simulations capture many aspects of the observed variations in streamflow and soil moisture, suggesting that they may be used to supplement available observations to study the interannual to multidecadal variations in surface runoff, soil moisture, and evaporation, whose historical records are sparse or unavailable. Future improvements to the forcing data, in particular with corrections for the undercatch and topography-induced biases in precipitation and increased resolution for regional modeling, as well as new developments in the CLM3 such as improved representations of the mean soil moisture content (e.g., by using more realistic soil layer depth and removing/routing subsurface runoff at a slower pace than surface runoff), routing of runoff (e.g., at higher than 0.5° resolution and including water balances of lakes, reservoirs, and wetlands), human influences on streamflow, and groundwater, are required for these models to be able to simulate past land surface conditions realistically.

Acknowledgments. We thank Sam Levis, Mariana Vertenstein, and Gordon Bonan for help with the CLM3 runs, Y.-C. Zhang for providing the ISCCP datasets, Beate Liepert for providing the GEBA datasets, Steve Yeager for help with NCAR DSS datasets, H.-L. Pan and W. Ebisuzaki of NCEP for helpful input, and three reviewers for their constructive comments that substantially improved the manuscript. NCEP–NCAR reanalysis data were partly from the NOAA–CIRES Climate Diagnostics Center Web site, http://www.cdc.noaa.gov/cdc/reanalysis/. This study was supported by NSF Grant ATM-0233568 and NCAR's Water Cycle Across Scales Initiative. The forcing dataset set is available from http://www.cgd.ucar.edu/cas/catalog/.

REFERENCES

Adam, J. C., and D. P. Lettenmaier, 2003: Adjustment of global gridded precipitation for systematic bias. *J. Geophys. Res.,* **108,** 4257, doi:10.1029/2002JD002499.

——, E. A. Clark, D. P. Lettenmaier, and E. F. Wood, 2006: Correction of global precipitation products for orographic effects. *J. Climate,* **19,** 15–38.

Adler, R. F., and Coauthors, 2003: The Version-2 Global Precipitation Climatology Project (GPCP) monthly precipitation analysis (1979–present). *J. Hydrometeor.,* **4,** 1147–1167.

Beck, C., J. Grieser, and B. Rudolf, 2005: A new monthly precipitation climatology for the global land areas for the period 1951 to 2000. Climate Status Report 2004, German Weather Service, 181–190.

Berezovskaya, S., D. Q. Yang, and D. L. Kane, 2004: Compatibility analysis of precipitation and runoff trends over the large Siberian watersheds. *Geophys. Res. Lett.,* **31,** L21502, doi:10.1029/2004GL021277.

Berg, A. A., J. S. Famiglietti, J. P. Walker, and P. R. Houser, 2003: Impact of bias correction to reanalysis products on simulations of North American soil moisture and hydrological fluxes. *J. Geophys. Res.,* **108,** 4490, doi:10.1029/2002JD003334.

Betts, A. K., J. H. Ball, and P. Viterbo, 2003: Evaluation of the ERA-40 surface water budget and surface temperature for the Mackenzie River basin. *J. Hydrometeor.,* **4,** 1194–1211.

——, ——, ——, A. Dai, and J. A. Marengo, 2005: Hydrometeorology of the Amazon from ERA-40. *J. Hydrometeor.,* **6,** 764–774.

Bonan, G. B., S. Levis, L. Kergoat, and K. W. Oleson, 2002a: Landscapes as patches of plant functional types: An integrating concept for climate and ecosystem models. *Global Biogeochem. Cycles,* **16,** 1021, doi:10.1029/2000GB001360.

——, K. W. Oleson, M. Vertenstein, S. Levis, X. Zeng, Y. Dai, R. E. Dickinson, and Z. Yang, 2002b: The land surface climatology of the Community Land Model coupled to the NCAR Community Climate Model. *J. Climate,* **15,** 3123–3149.

Bowling, L. C., D. P. Lettenmaier, B. Nijssen, J. Polcher, R. D. Koster, and D. Lohmann, 2003: Simulation of high latitude hydrological processes in the Torne-Kalix basin: PILPS Phase 2(e) 3: Equivalent model representation and sensitivity experiment. *J. Global Planet. Change,* **38,** 55–71.

Chen, M., P. Xie, J. E. Janowiak, and P. A. Arkin, 2002: Global land precipitation: A 50-yr monthly analysis based on gauge observations. *J. Hydrometeor.,* **3,** 249–266.

Cullather, R. I., D. H. Bromwich, and M. C. Serreze, 2000: The atmospheric hydrologic cycle over the Arctic Basin from reanalyses. Part I: Comparison with observations and previous studies. *J. Climate,* **13,** 923–937.

Dai, A., 2001a: Global precipitation and thunderstorm frequencies. Part I: Seasonal and interannual variations. *J. Climate,* **14,** 1092–1111.

——, 2001b: Global precipitation and thunderstorm frequencies. Part II: Diurnal variations. *J. Climate,* **14,** 1112–1128.

——, 2006: Recent climatology, variability, and trends in global surface humidity. *J. Climate,* **19,** 3589–3606.

——, and K. E. Trenberth, 2002: Estimates of freshwater discharge from continents: Latitudinal and seasonal variations. *J. Hydrometeor.,* **3,** 660–687.

——, and ——, 2004: The diurnal cycle and its depiction in the Community Climate System Model. *J. Climate,* **17,** 930–951.

——, I. Y. Fung, and A. D. Del Genio, 1997: Surface observed global land precipitation variations during 1900–88. *J. Climate,* **10,** 2943–2962.

——, K. E. Trenberth, and T. Qian, 2004: A global data set of Palmer Drought Severity Index for 1870–2002: Relationship with soil moisture and effects of surface warming. *J. Hydrometeor.,* **5,** 1117–1130.

——, A. Hu, G. A. Meehl, W. M. Washington, and W. G. Strand, 2005: Atlantic thermohaline circulation in a coupled model: Unforced variations versus forced changes. *J. Climate,* **18,** 2990–3013.

——, T. R. Karl, B. Sun, and K. E. Trenberth, 2006: Recent trends in cloudiness over the United States: A tale of monitoring inadequacies. *Bull. Amer. Meteor. Soc.,* **87,** 597–606.

Dai, Y., and Coauthors, 2003: The Common Land Model. *Bull. Amer. Meteor. Soc.,* **84,** 1013–1023.

Dickinson, R. E., K. W. Oleson, G. B. Bonan, F. Hoffman, P. Thornton, M. Vertenstein, Z.-L. Yang, and X. Zeng, 2006:

The Community Land Model and its climate statistics as a component of the Community Climate System Model. *J. Climate,* **19,** 2302–2324.

Dirmeyer, P. A., and L. Tan, 2001: A multi-decadal global land-surface data set of state variables and fluxes. COLA Tech. Rep. 102, 43 pp. [Available from COLA, 4041 Powder Mill Rd., #302, Calverton, MD 20705.]

——, A. J. Dolman, and N. Sato, 1999: The Global Soil Wetness Project: A pilot project for global land surface modeling and validation. *Bull. Amer. Meteor. Soc.,* **80,** 851–878.

Dobson, F. W., and S. D. Smith, 1988: Bulk models of solar-radiation at sea. *Quart. J. Roy. Meteor. Soc.,* **114,** 165–182.

Entin, J., A. Robock, K. Y. Vinnikov, S. Qiu, V. Zabelin, S. Liu, A. Namkhai, and T. Adyasuren, 1999: Evaluation of Global Soil Wetness Project soil moisture simulations. *J. Meteor. Soc. Japan,* **77,** 183–198.

Fan, Y., and H. M. Van den Dool, 2004: Climate Prediction Center global monthly soil moisture data set at 0.5° resolution for 1948 to present. *J. Geophys. Res.,* **109,** D10102, doi:10.1029/2003JD004345.

——, ——, K. E. Mitchell, and D. Lohmann, 2003: A 51-year reanalysis of the U.S. land-surface hydrology. *GEWEX News,* No. 13, International GEWEX Project Office, Silver Spring, MD, 6–10.

Fekete, B. M., C. J. Vörösmarty, and W. Grabs, 2000: Global composite runoff fields based on observed river discharge and simulated water balances. Global Runoff Data Centre Rep. 22, Koblenz, Germany, 39 pp. + annex. [Available online at www.bafg.de/grdc.htm.]

——, ——, and ——, 2002: High resolution fields of global runoff combining observed river discharge and simulated water balances. *Global Biogeochem. Cycles,* **16,** 1042, doi:10.1029/1999GB001254.

Gilgen, H., M. Wild, and A. Ohmura, 1998: Means and trends of shortwave irradiance at the surface estimated from global energy balance archive data. *J. Climate,* **11,** 2042–2061.

Hansen, J., R. Ruedy, M. Sato, M. Imhoff, W. Lawrence, D. Easterling, T. Peterson, and T. Karl, 2001: A closer look at United States and global surface temperature change. *J. Geophys. Res.,* **106,** 23 947–23 963.

Higgins, R. W., K. C. Mo, and S. D. Schubert, 1996: The moisture budget of the central United States as evaluated in the NCEP/NCAR and the NASA/DAO reanalyses. *Mon. Wea. Rev.,* **124,** 939–963.

Hollinger, S. E., and S. A. Isard, 1994: A soil moisture climatology of Illinois. *J. Climate,* **7,** 822–833.

Houghton, J. T., Y. Ding, D. J. Griggs, M. Noguer, P. J. van der Linden, and D. Xiaosu, Eds., 2001: *Climate Change 2001: The Scientific Basis*. Cambridge University Press, 944 pp.

Huang, J., H. M. Van den Dool, and K. P. Georgakakos, 1996: Analysis of model-calculated soil moisture over the United States (1931–1993) and applications to long-range temperature forecasts. *J. Climate,* **9,** 1350–1362.

Janowiak, J. E., A. Gruber, C. R. Kondragunta, R. E. Livezy, and G. J. Huffman, 1998: A comparison of the NCEP–NCAR reanalysis precipitation and the GPCP rain gauge–satellite combined dataset with observational error considerations. *J. Climate,* **11,** 2960–2979.

Jones, P. D., and A. Moberg, 2003: Hemispheric and large-scale surface air temperature variations: An extensive revision and an update to 2001. *J. Climate,* **16,** 206–223.

Kalnay, E., and Coauthors, 1996: The NCEP/NCAR 40-Year Reanalysis Project. *Bull. Amer. Meteor. Soc.,* **77,** 437–471.

Kistler, R., and Coauthors, 2001: The NCEP–NCAR 50-year reanalysis: Monthly means CD-ROM and documentation. *Bull. Amer. Meteor. Soc.,* **82,** 247–267.

Legates, D. R., D. Yang, S. Quiring, K. Freeman, and T. Bogart, 2005: Bias adjustments to Arctic precipitation: A comparison of daily versus monthly bias adjustments. Preprints, *Eighth Conf. on Polar Meteorology and Oceanography,* San Diego, CA, Amer. Meteor. Soc., CD-ROM, 5.1.

Lenters, J. D., M. T. Coe, and J. A. Foley, 2000: Surface water balance of the continental United States, 1963–1995: Regional evaluation of a terrestrial biosphere model and the NCEP/NCAR reanalysis. *J. Geophys. Res.,* **105,** 22 393–22 425.

Maurer, E. P., G. M. O'Donnell, D. P. Lettenmaier, and J. O. Roads, 2001: Evaluation of the land surface water budget in NCEP/NCAR and NCEP/DOE reanalyses using an off-line hydrologic model. *J. Geophys. Res.,* **106,** 17 841–17 862.

——, A. W. Wood, J. C. Adam, D. P. Lettenmaier, and B. Nijssen, 2002: A long-term hydrologically based dataset of land surface fluxes and states for the conterminous United States. *J. Climate,* **15,** 3237–3251.

McClelland, J. W., R. M. Holmes, B. J. Peterson, and M. Stieglitz, 2004: Increasing river discharge in the Eurasian Arctic: Consideration of dams, permafrost thaw, and fires as potential agents of change. *J. Geophys. Res.,* **109,** D18102, doi:10.1029/2004JD004583.

Mitchell, K. E., and Coauthors, 2004: The multi-institution North American Land Data Assimilation System (NLDAS): Utilizing multiple GCIP products and partners in a continental distributed hydrological modeling system. *J. Geophys. Res.,* **109,** D07S90, doi:10.1029/2003JD003823.

Nakamura, M., 1996: Effects of ice albedo and runoff feedbacks on the thermohaline circulation. *J. Climate,* **9,** 1783–1794.

New, M., M. Hulme, and P. Jones, 1999: Representing twentieth-century space–time climate variability. Part I: Development of a 1961–90 mean monthly terrestrial climatology. *J. Climate,* **12,** 829–856.

——, ——, and ——, 2000: Representing twentieth-century space–time climate variability. Part II: Development of 1901–96 monthly grids of terrestrial surface climate. *J. Climate,* **13,** 2217–2238.

——, D. Lister, M. Hulme, and I. Makin, 2002: A high-resolution data set of surface climate for terrestrial land areas. *Climate Res.,* **21,** 1–25.

Ngo-Duc, T., J. Polcher, and K. Laval, 2005: A 53-year forcing data set for land surface models. *J. Geophys. Res.,* **110,** D06116, doi:10.1029/2004JD005434.

Nijssen, B., G. M. O'Donnell, D. P. Lettenmaier, D. Lohmann, and E. F. Wood, 2001a: Predicting the discharge of global rivers. *J. Climate,* **14,** 3307–3323.

——, R. Schnur, and D. P. Lettenmaier, 2001b: Global retrospective estimation of soil moisture using the Variable Infiltration Capacity land surface model, 1980–1993. *J. Climate,* **14,** 1790–1808.

——, and Coauthors, 2003: Simulation of high latitude hydrological processes in the Torne-Kalix basin: PILPS Phase 2(e) 2: Comparison of model results with observations. *Global Planet. Change,* **38,** 31–53.

Oleson, K. W., and Coauthors, 2004: Technical description of the community land model (CLM). NCAR Tech. Note NCAR/TN-461+STR, 186 pp. [Available online at http://www.cgd.ucar.edu/tss/clm/distribution/clm3.0/TechNote/CLM_Tech_Note.pdf.]

Roads, J., and A. Betts, 2000: NCEP/NCAR and ECMWF reanalysis surface water and energy budgets for the Mississippi River basin. *J. Hydrometeor.,* **1,** 88–94.

Robock, A., C. A. Schlosser, K. Y. Vinnikov, N. A. Speranskaya, J. K. Entin, and S. Qiu, 1998: Evaluation of AMIP soil moisture simulations. *Global Planet. Change,* **19,** 181–208.

——, K. Y. Vinnikov, G. Srinivasan, J. K. Entin, S. E. Hollinger, N. A. Speranskaya, S. Liu, and A. Namkhai, 2000: The Global Soil Moisture Data Bank. *Bull. Amer. Meteor. Soc.,* **81,** 1281–1299.

Rodell, M., and Coauthors, 2004: The Global Land Data Assimilation System. *Bull. Amer. Meteor. Soc.,* **85,** 381–394.

Ruiz-Barradas, A., and S. Nigam, 2005: Warm-season rainfall variability over the U.S. Great Plains in observations, NCEP and ERA-40 reanalyses, and NCAR and NASA atmospheric model simulations: Intercomparisons for NAME. *J. Climate,* **18,** 1808–1830.

Serreze, M. C., and C. M. Hurst, 2000: Representation of mean Arctic precipitation from NCEP–NCAR and ERA reanalyses. *J. Climate,* **13,** 182–201.

Sheffield, J., A. D. Ziegler, E. F. Wood, and Y. Chen, 2004: Correction of the high-latitude rain day anomaly in the NCEP/NCAR reanalysis for land surface hydrological modeling. *J. Climate,* **17,** 3814–3828.

Shiklomanov, A. I., R. B. Lammers, and C. J. Vörösmarty, 2002: Widespread decline in hydrological monitoring threatens pan-Arctic research. *Eos, Trans. Amer. Geophys. Union,* **83,** 13–16.

Thornton, P. E., and S. W. Running, 1999: An improved algorithm for estimating incident daily solar radiation from measurements of temperature, humidity, and precipitation. *Agric. For. Meteor.,* **93,** 211–228.

Trenberth, K. E., 2004: Rural land-use change and climate. *Nature,* **427,** 213–214.

——, and C. J. Guillemot, 1998: Evaluation of the atmospheric moisture and hydrological cycle in the NCEP/NCAR reanalysis. *Climate Dyn.,* **14,** 213–231.

——, J. M. Caron, and D. P. Stepaniak, 2001a: The atmospheric energy budget and implications for surface fluxes and ocean heat transports. *Climate Dyn.,* **17,** 259–276.

——, D. P. Stepaniak, J. W. Hurrell, and M. Fiorino, 2001b: Quality of reanalyses in the Tropics. *J. Climate,* **14,** 1499–1510.

——, A. Dai, R. M. Rasmussen, and D. B. Parsons, 2003: The changing character of precipitation. *Bull. Amer. Meteor. Soc.,* **84,** 1205–1217.

Uppala, S. M., and Coauthors, 2005: The ERA-40 reanalysis. *Quart. J. Roy. Meteor. Soc.,* **131,** 2961–3012.

Van den Dool, H., J. Huang, and Y. Fan, 2003: Performance and analysis of the constructed analogue method applied to U.S. soil moisture over 1981–2001. *J. Geophys. Res.,* **108,** 8617, doi:10.1029/2002JD003114.

Vinnikov, K., and I. B. Yeserkepova, 1991: Soil moisture: Empirical data and model results. *J. Climate,* **4,** 66–79.

Yang, D., B. Ye, and D. Kane, 2004: Streamflow hydrology changes over Siberian Yenisei river basin. *J. Hydrol.,* **296,** 59–80.

Zeng, X., M. Shaikh, Y. Dai, R. E. Dickinson, and R. Myneni, 2002: Coupling of the Common Land Model to the NCAR Community Climate Model. *J. Climate,* **15,** 1832–1854.

Zhang, Y.-C., W. B. Rossow, A. A. Lacis, V. Oinas, and M. I. Mishchenko, 2004: Calculation of radiative fluxes from the surface to top of atmosphere based on ISCCP and other global data sets: Refinements of the radiative transfer model and the input data. *J. Geophys. Res.,* **109,** D19105, doi:10.1029/2003JD004457.

Ziegler, A. D., J. Sheffield, E. F. Wood, E. P. Maurer, B. Nijssen, and D. P. Lettenmaier, 2002: Detection of an acceleration in the global water cycle: The potential role of FRIEND. *FRIEND 2002—Regional Hydrology: Bridging the Gap between Research and Practice,* H. A. J. van Lanen and S. Demuth, Eds., IAHS Series of Proceedings and Reports, No. 274, International Association of Hydrological Sciences, 51–57.